Eur Biophys J
DOI 10.1007/s00249-017-1256-0

ORIGINAL ARTICLE

Intrinsic thermodynamics of high affinity inhibitor binding to recombinant human carbonic anhydrase IV

Aurelija Mickevičiūtė[1] · David D. Timm[1] · Marius Gedgaudas[1] · Vaida Linkuvienė[1] · Zhiwei Chen[2] · Abdul Waheed[2] · Vilma Michailovienė[1] · Asta Zubrienė[1] · Alexey Smirnov[1] · Edita Čapkauskaitė[1] · Lina Baranauskienė[1] · Jelena Jachno[1] · Jurgita Revuckienė[1] · Elena Manakova[3] · Saulius Gražulis[3] · Jurgita Matulienė[1] · Enrico Di Cera[2] · William S. Sly[2] · Daumantas Matulis[1]

Received: 5 July 2017 / Revised: 7 September 2017 / Accepted: 15 September 2017

Abstract Membrane-associated carbonic anhydrase (CA) isoform IV participates in carbon metabolism and pH homeostasis and is implicated in the development of eye diseases such as retinitis pigmentosa and glaucoma. A series of substituted benzenesulfonamides were designed and their binding affinity to CA IV was determined by fluorescent thermal shift assay and isothermal titration calorimetry (ITC). Compound [(4-chloro-2-phenylsulfanyl-5-sulfamoyl-benzoyl)amino]propyl acetate (**19**) bound CA IV with the K_d of 1.0 nM and exhibited significant selectivity over the remaining 11 human CA isoforms. The compound could be developed as a drug targeting CA IV. Various forms of recombinant CA IV were produced in *Escherichia coli* and mammalian cell cultures. Comparison of their temperature stability in various buffers and salt solutions demonstrated that CA IV is most stable at slightly alkaline conditions and at elevated sodium sulfate concentrations. High-resolution X-ray crystallographic structures of ortho-Cl and meta-thiazole-substituted benzene sulfonamide in complex with CA IV revealed the position of and interactions between the ligand and the protein. Sulfonamide inhibitor binding to CA IV is linked to several reactions—the deprotonation of the sulfonamide amino group, the protonation of CA–Zn(II)-bound hydroxide at the active site of CA IV, and the compensating reactions of the buffer. The dissection of binding-linked reactions yielded the intrinsic thermodynamic parameters, characterizing the interaction between CA IV and the sulfonamides in the binding-able protonation forms, including Gibbs energy, enthalpy, and entropy, that could be used for the characterization of binding to any CA in the process of drug design.

Keywords Carbonic anhydrase · Isothermal titration calorimetry · Fluorescent thermal shift assay · Differential scanning fluorimetry · Intrinsic thermodynamics of protein–ligand binding · X-ray crystallography

Abbreviations

AZM	Acetazolamide (also abbreviated as AAZ, ACTAZ)
BSA	Benzenesulfonamide
CA	Carbonic anhydrase
CA IV	Isozyme 4 of the human carbonic anhydrase protein family
EZA	Ethoxzolamide
FTSA	Fluorescent thermal shift assay
ITC	Isothermal titration calorimetry
MZM	Methazolamide (also METHZ)
PAMBS	Para-aminomethyl-benzenesulfonamide
TFS	Trifluoromethane sulfonamide (also TFMSA)
TPM	Topiramate

Introduction

Carbonic anhydrases (CAs) are metalloenzymes that catalyze the reversible hydration of CO_2 into bicarbonate and protons and thus are essential to maintaining intracellular

✉ Daumantas Matulis
matulis@ibt.lt; daumantas.matulis@bti.vu.lt

[1] Department of Biothermodynamics and Drug Design, Institute of Biotechnology, Life Sciences Center, Vilnius University, Saulėtekio 7, 10257 Vilnius, Lithuania

[2] Department of Biochemistry and Molecular Biology, Saint Louis University School of Medicine, St. Louis, MO 63104, USA

[3] Department of Protein-DNA Interactions, Institute of Biotechnology, Life Sciences Center, Vilnius University, Saulėtekio 7, 10257 Vilnius, Lithuania

Published online: 03 October 2017

and extracellular pH. CAs are found in all three domains of life and belong to several different families: α, β, γ, δ, ζ, η and θ (Zolfaghari Emameh et al. 2016a, b; Kikutani et al. 2016). α-CAs are found in many organisms, including fungi (together with β-CAs) (Elleuche and Pöggeler 2010). β-CAs are also found in plants, archaea, and both eukaryotes and prokaryotes (Supuran 2004). γ-CAs are found in bacteria (Ferry 2010). δ-CAs and ζ-CAs arefound in certain marine planktonic species (Lane et al. 2005). η-CAs are found in *Plasmodium falciparum*, malaria causative agent (Del Prete et al. 2014). θ-CAs are found in marine diatom *Phaeodactylum tricornutum* (Kikutani et al. 2016). Most CAs have zinc(II) ions in their active center, though some can have cadmium, iron or cobalt (Lane et al. 2005, Ferry 2010).

Human CAs belong to the α-CA family and are zinc-containing metalloenzymes. Humans have 15 CA isoforms but only 12 of them contain Zn(II) and are catalytically active. Each isoform has somewhat different kinetic properties and inhibitor affinity profiles, and may be located in different tissues. In the cell, different CAs can be located in the cytosol (CA I, CA II, CA III, CA VII, and CA XIII), in mitochondria (CA VA and CA VB), or on the cell membrane (CA IV, CA IX, CA XII, and CA XIV), or be secreted in saliva and milk (CA VI) (Purkerson and Schwartz 2007; Liu et al. 2012). These enzymes are important not only for pH maintenance, but also for signal transduction, bone resorption, calcification, renal acidification, gluconeogenesis, gastric acid formation, metabolism, adaptation to cellular stress, biosynthesis, and other processes (Breton 2001; Kivelä et al. 2005; Krishnamurthy et al. 2008).

CA IV is the most widely distributed of all membrane-associated CA isoforms and has a unique glycosylphosphatidylinositol anchor that attaches it to the membrane in the outer surface (Purkerson and Schwartz 2007). This anchor may also activate the protein. It is also known that CA IV can be activated by small concentrations (< 20 mM) of chloride, bromide, and phosphate (Baird et al. 1997) and it was the first discovered membrane–associated CA (Datta et al. 2010). The CA IV propeptide length is 312 amino acids and the MW is about 35 kDa (Kivelä et al. 2005). Human CA IV is physiologically stabilized by two disulphide bonds between Cys24–Cys36 and Cys46–Cys229 (Waheed et al. 1996). These bonds make CA IV stable, for example, in the presence of 5% SDS, while CA II is deactivated in these conditions (Baird et al. 1997). CA IV is widely distributed in the human body, including kidneys, lungs, colon, pancreas cell plasma membranes, eye and brain capillaries, nasal mucosa, esophageal epithelium, salivary glands, and heart muscle (Pastorekova et al. 2004; Supuran 2004; Purkerson and Schwartz 2007; Datta et al. 2009). CA IV is the most important protein for HCO_3^- resorption in kidneys (Sterling et al. 2002). CA II and CA IV are part of the bicarbonate transport metabolon. Maintaining pH is very important and malfunction of this metabolon correlates with some diseases (McMurtrie et al. 2004). CA IV catalyses CO_2 exchange in lungs and the hydration of CO_2 that is produced in muscle during exercise (Waheed et al. 1996). Together with CA XIV, CA IV is the main CA in the brain extracellular space that maintains pH homeostasis. CA XIV and CA IV also maintain intracellular pH in the hippocampal neurons (Svichar et al. 2009). Together with CA II, CA IV participates in compacting of myelin membranes, but CA IV alone is not sufficient to keep myelin compact (Cammer et al. 1995). CA I–IV are found in esophageal epithelium where, among other functions, they protect against gastric acid reflux (Christie et al. 1997).

CA IV plays a role in the development of several diseases, such as retinitis pigmentosa and glaucoma. Retinitis pigmentosa, an inherited progressive eye disease, results in blindness at the age of 40–50 years. Retinitis pigmentosa affects one in 3000–7000 people, both men and women (Köhn et al. 2008; Datta et al. 2009; Ferrari et al. 2011). In these patients, CA IV carries the R14W mutation and the mutated protein cannot maintain the pH homeostasis, causing the photoreceptors to degenerate due to apoptosis (Yang et al. 2005). Recently it was shown that CA IV plays a very important role in suppressing colorectal cancer and in wound healing (Zhang et al. 2016). After injury, CA IV expression is induced by inflammation and, together with CA IX, it generates an acidic micro-environment, crucial for neutrophil survival and keratynocyte migration (Barker et al. 2017). CA IV and CA III functions might be altered in rheumatoid arthritis, systemic lupus erythematosus, type 1 and 2 diabetic nephropathy, type 1 and 2 diabetes, and heart failure, since high titers of anti–CA III and/or anti–CA IV antibodies were found in the serum of people affected by these diseases (Liu et al. 2012). There are also antibodies to CA IV in the serum of people diagnosed with autoimmune pancreatitis and Sjögren's syndrome (Nishimori et al. 2005).

CA IV is one of the most enzymatically active CA isoforms. Its k_{cat} for CO_2 hydration is 1.1×10^6 s^{-1} while the CA II k_{cat} is 8×10^5 s^{-1}. CA IV is also more active in HCO_3^- dehydration than CA II (Baird et al. 1997). CA IV is inhibited by bromophenol compounds (Balaydin et al. 2012). It is also inhibited by acetazolamide (AZM), ethoxzolamide (EZA), and bromosulfanilamide. Celecoxib and some halogenated sulfanilamides are also inhibitors of medium potency. CA IV is located outside the cell. Therefore, it can be selectively inhibited by positively charged sulfonamides that cannot cross the plasma membrane (Supuran 2008). Since CA IV is involved in many processes, selective inhibitors might have clinical importance (Innocenti et al. 2005).

The crystal structure of the secretory form of human CA IV was first determined by Stams et al. (Stams et al. 1996). A unique loop on the opposite side of the active site, the Val-131-Asp-136 segment, was found to be specific to this

isozyme instead of the alpha-helix conformation found in other isozymes.

We have designed a series of 35 novel substituted benzenesulfonamides and have discovered a compound **19** (3-[(4-chloro-2-phenylsulfanyl-5-sulfamoyl-benzoyl)amino] propyl acetate) that bound CA IV with the K_d of 1.0 nM and had significant selectivity towards this isoform over other human CA isoforms. The high-resolution crystal structure for compound **20** in complex with CA IV revealed the most important interactions between the ligand and protein.

A detailed thermodynamic analysis of EZA and trifluormethanesulfonamide (TFS) binding to CA IV was performed by isothermal titration calorimetry (ITC) and fluorescent thermal shift assay (FTSA) to determine the intrinsic thermodynamics of compound binding. Intrinsic values do not depend on pH or buffer because they take into account the binding-linked protonation reactions, while direct determinations of binding or inhibition by any enzymatic or biophysical techniques always yield the observed dissociation constants that should not be directly used to correlate the structure with thermodynamics. The pH dependence of the binding affinities and the observed enthalpies of binding enabled us to obtain the pK_a and the enthalpy of protonation of the Zn bound water at the active site of CA IV. These values should help other researchers to determine the *intrinsic* thermodynamics of binding to CA IV and develop drugs targeting CA IV.

Results and discussion

Observed thermodynamics of ligand binding to CA IV

The binding affinity of a novel series of substituted benzenesulfonamides **1**–**35** (Fig. 1) to CA IV was determined by FTSA. The compounds that bind to the active site of CA IV stabilized the protein and shifted the protein melting temperature (T_m) upward (Fig. 2). The observed dissociation constants ($K_{d\text{-obs}}$) were obtained after the simulation or regression of the ligand-dosing curve according to the model (Cimmperman et al. 2008). According to the data in Table 1, many compounds showed better affinities for CA IV than the non-substituted compound benzenesulfonamide (BSA). Tetrafluorbenzenesulfonamide derivatives **1**–**10** bearing substitutions at the *para* position bound CA IV with $K_{d\text{-obs}}$ ranging from 50 to 830 nM. The introduction of ortho substituent (compounds **11**–**15**) resulted in much weaker binding to CA IV ($K_{d\text{-obs}}$ in the range of 400–4000 nM). However, meta substituted derivatives **17**–**18** bearing a short hydroxyethylthio group at the *para* position had higher binding affinities ($K_{d\text{-obs}}$ 17–18 nM). For the series of **19**–**35** compounds, compound **19** was the most potent binder of CA IV, with an extraordinary $K_{d\text{-obs}}$ of 1 nM.

For analysis of the selectivity, we tested the binding of five selected compounds toward all CA isoforms and compared the data with BSA and AZM (Table 2). Compound **5** was a selective and high-affinity binder of CA I and CA VB ($K_{d\text{-obs}}$ in the low nanomolar range), and had a lower affinity to CA IV and CA VA ($K_{d\text{-obs}}$ in the range 170–100 nM). Compounds **18**, **19,** and **26** bound CA IV 28, 4000, and 23-times stronger, respectively, than CA I, one of the most abundant isoforms found in the human organism. However, their binding affinity to CA VII, CA IX, CA XII, CA XIII, and CA XIV was higher or similar to CA IV. Compound **19** was selective toward CA IV, bound CA IV 4000 times stronger than CA I and 10 times stronger than CA II. This compound, or compounds with similar structures, may be developed as drugs targeting CA IV.

Crystal structure of CA IV in complex with inhibitors

The crystal structures of human CA IV in complex with the synthesized compound **20** and five commercially available CA inhibitors, namely EZA, AZM, methazolamide (MZM), 4-aminomethylbenzenesulfonamide chloride (PAMBS) and topiramate (TPM), were determined by X-ray crystallography. Data collection and refinement statistics are shown in Table 3. The quality of electron densities for the complexes of compound **20** and five other inhibitors is shown in Fig. 3, parts b1–b6. For the complex with compound **20**, the asymmetric unit of the crystal structure contains four subunits. Three sets of electron densities attributable to the inhibitor were found in protein chains A, B, and C. The location of the compound is nearly identical in all three protein chains with small differences in the positions of the second ring.

The location of the 2-chlorobenzenesulfonamide ring in the active site of several human CA isoforms (CA XII, CA XIII, and CA II) described earlier (Čapkauskaitė et al. 2013) is very similar. The chlorine atom is anchored in a hydrophobic pocket formed by the residues conserved between human CA isoforms (in CA II Val121, Leu141, Val143, and Leu198). On the other hand, the active site of CA IV is more hydrophilic (Fig. 3c1), but the hydrophilic residues do not interact with inhibitor **20**. The dissociation constants of compound **20** with CA IV and CA II are very similar (200 and 290 nM, respectively, Table 2). The dissociation constants of **20** with CA XII and CA XIII are also very similar (330 and 100 nM accordingly, Table 2). These values can reflect similar interaction of **20** with these CA isoforms (Fig. 3a1), since a relatively simple compound interacts with the most conserved part of the CA binding site.

The buried surface area (in $Å^2$) calculated by PISA v1.06 (Krissinel and Henrick 2007) values of the side chains that interact with **20** for protein chain A are given in Table 4. The

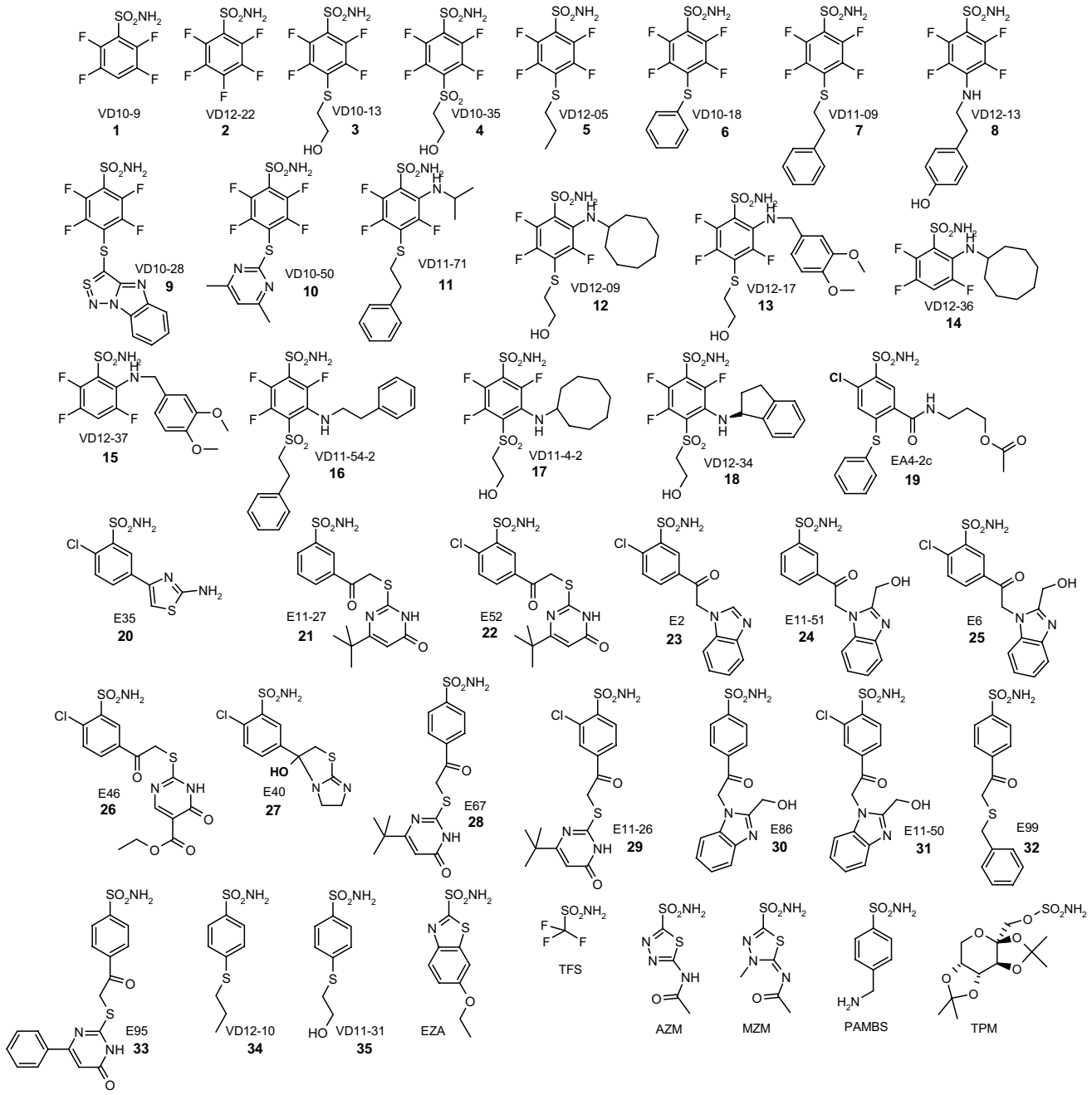

Fig. 1 The structures of synthesized compounds **1–35** and six conventional CA inhibitors EZA, TFS, AZM, MZM, PAMBS, and TPM, that were used in this study

largest buried surface area values contain residues Asn69, Met74, Gln96, His98, Leu207, and Thr209. Most of these residues are present both in CA IV and CA II isoforms, except for Phe131 in CA II, which does not have a structural counterpart in the crystal structures of CA IV, and Met74 in CA IV, which coincides spatially with Asn67 in CA II.

In the protein chain A of CA IV, an electron density was found, corresponding to residues Lys128–Gln140, that was absent in other protein chains of PDB ID 5IPZ as well as in other CA IV crystal structures (except PDB ID 1ZNC, 2.8 Å) (Stams and Christianson 2000; Vernier et al. 2010). Despite the poor quality of the electron map, we were able to put most of the residues into the protein model. The flexible loop interacts with the surface of the symmetric equivalent of the protein chain B, and it is likely that such a conformation reflects an artifact of the crystal packing. Interestingly, the residues that correspond to this loop are quite well fixed in CAII (residues 127–137) (Fig. 3a2) and form part of the

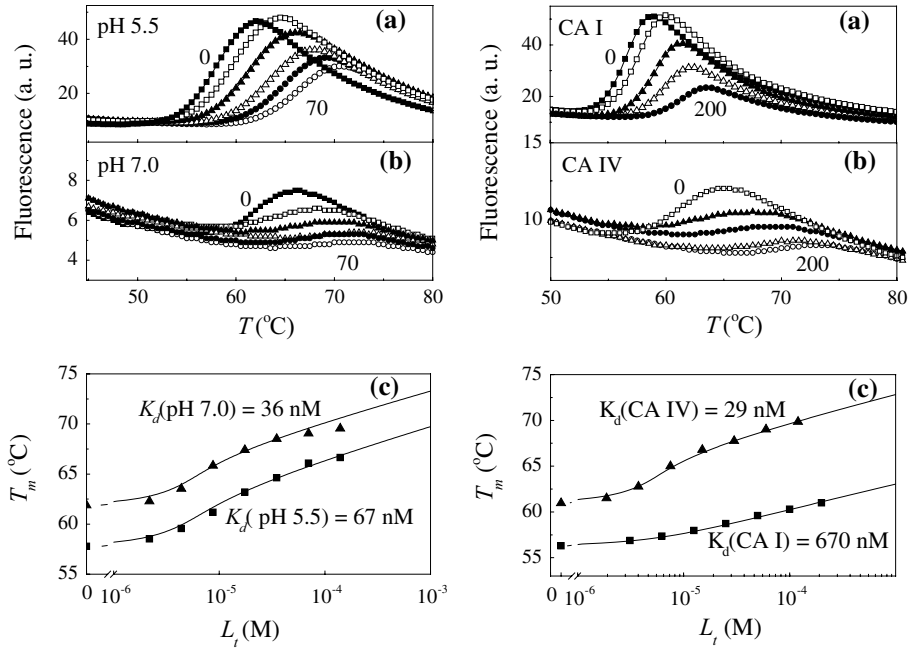

Fig. 2 Fluorescent thermal shift assay data of EZA (left) binding to CA IV and compound **26** (right) binding to CA I and CA IV. Left panels a-b show the thermal melting fluorescence curves of CA IV (10 μM) in the universal buffer, pH 5.5 and 7.0, in the presence of various EZA concentrations, 0 μM (filled square), 4.4 μM (open square), 8.8 μM (filled triangle), 17.5 μM (open triangle), 35 μM (filled circle), and 70 μM (open circle). Right panels **a**, **b** show the thermal melting fluorescence curves of CA I (5 μM) and CA IV (10 μM) in phosphate buffer, pH 7.0, in the presence of various compound **26** concentrations, 0 μM (filled square), 12 μM (open square), 50 μM (filled triangle), 100 μM (open triangle), and 200 μM (open circle). Panels **c** show the ligand dosing curves plotting the melting temperatures (T_m) from data in panels **a**, **b** as a function of added compound concentration. The lines were regressed according to (Cimmperman et al. 2008)

active site in CA II. Phe131, which is often involved in the interaction with sulfonamide inhibitors, is also located in this region.

For the complexes with AZM, EZA, TPM, PAMBS, and MZM, crystals were grown in space group $p2_12_12_1$, with almost identical unit cells containing four molecules in the asymmetric unit (Table 3). The structures of the CA molecules A, B, C, and D including inhibitors were very similar, with the rms deviation of ~0.2 Å for these five complexes. However, residues 126–138 (using the numbering of CA II) in molecules A and B were disordered while residues 126–138 in molecule C and D were ordered and visible in the electron density map. Comparing the structures of molecule C in the complex of CA IV and AZM, molecule A of PDB ID 1ZNC, the first crystal structure of human CA IV where the residues 126–138 in molecule B were disordered (Stams et al. 1996), molecule A in complex of human CA IV and compound 20, and human CA II (PDB ID 4HT0) (Fig. 3a2), showed that the orientation of residues 126–138 in CA IV differs greatly from CA II. The structure of residues 126–138 in CA II is very similar with that of another CA family, in which residue 131 was an important residue located in a short helix and interacted with inhibitors in most isoforms of the CA family. This helix acts as a lid and closes the active site pocket in CA II. The structures of residues 126–138 in human CA IV were very flexible and there were four different conformations (including the disordered one) in the segment found so far. Although the conformations in this region were different, all of them made the active site pocket bigger and allowed larger inhibitors to interact with the active site.

The active site structure in the complex of human CA IV and inhibitor consisted of a metal binding site, protein ligands from the nitrogen atoms of His94, His96, and His119 as well as the nitrogen atom from the inhibitor, a hydrophobic pocket containing the residues Val121,Val143, Ile141, Val207, Trp209, and Leu198, and a hydrophilic pocket consisting of Tyr7, Asn62, His64, Ser65, Met67, Gln92, Thr199, and Thr200. Figure 3, parts c1, c2, c3, c4, c5, and c6, shows the interactions between inhibitors and the protein in the active site areas. All inhibitors formed two hydrogen bonds with the nitrogen atom from the main chain and the oxygen atom from the side chain of Thr199, which is a catalytic residue in CA IV. Residue His64 from the hydrophilic pocket is a proton shuttle in catalysis (Stams et al. 1996). Gly-63- → Gln substitution in rodent CA IV revealed the importance of residue His64 as a proton shuttle (Tamai et al. 1996). In fact, the complex structure of CA IV and AZM in

Table 1 The tested compound affinities to CA IV, determined by the fluorescent thermal shift assay at pH 7.0 and 25 °C

Compound	Compound lab name	pK_a	K_{d_obs} (nM)	K_{d_intr} (nM)
1	VD10-9	8.3	260	4.5
2	VD12-22	8.4	250	3.4
3	VD10-13	8.3	170	2.9
4	VD10-35	7.4	830	85
5	VD12-05	8.3	170	2.9
6	VD10-18	8.0	100	3.3
7	VD11-9	8.2	220	4.7
8	VD12-13	8.8	110	0.62
9	VD10-28	7.9	50	2.0
10	VD10-50	8.2	770	16
11	VD11-71	8.8	3300	19
12	VD12-09	8.8	400	2.2
13	VD12-17	8.8	3300	19
14	VD12-36	8.9	400	1.8
15	VD12-37	8.8	4000	22
16	VD11-54-2	8.1	670	18
17	VD11-4-2	8.2	17	0.36
18	VD12-34	8.0	18	0.59
19	EA4-2c	9.0	1.0	0.0036
20	E35	8.9	200	0.89
21	E11-27	9.4	6300	8.9
22	E52	8.9	140	0.64
23	E2	9.0	140	0.51
24	E11-51	9.5	50	0.064
25	E6	9.0	440	1.5
26	E46	8.9	29	0.13
27	E40	8.9	40	0.18
28	E67	9.4	133	0.19
29	E11-26	8.9	460	2.0
30	E86	9.1	330	0.95
31	E11-50	8.6	330	2.9
32	E99	9.4	16	0.023
33	E95	9.4	125	0.18
34	VD12-10	10.5	500	0.057
35	VD11-31-2	10.2	670	0.15
	BSA	10.0	5600	2.0
	EZA	8.0	16.2	0.40
	TFS	6.3	118	35
	AZM	7.3	50	6.0
	MZM	7.1	143	23
	PAMBS	10.1	3300	1.0
	TPM	8.7	45	0.32

The observed values were determined experimentally while the intrinsic affinities were calculated according to Eq. (1)

molecule A showed two conformations for the side chain of His64; one of them directed toward the active site and further certified the importance for this residue in CA IV. It was also observed that there were two conformations for the side chains of His64 in some crystal structures of CA II and CA VII. For the active site structure for compound **20** in complex with CA IV, there were no other interactions between the inhibitors and protein for the structures with EZA and PAMBS in CA IV (Fig. 3c3, c5), which revealed the most important hydrophobic interactions between the ligand and the protein. However, in the active site structure of CA IV with TPM, there were six hydrogen bonds in total between TPM and the hydrophilic residues. This bonding was attributed to the more hydrophilic oxygen atoms in TPM and provided a guide for designing new inhibitors with improved binding selectivity towards CA IV. Unfortunately, the crystal structure of **19** with CA IV was not obtained. This structure could have revealed the structural features of the lead compound, but the crystallization procedure was unsuccessful.

Determination of pK_a of Zn-bound water molecule in the active site of CA IV

The pK_a and enthalpy of protonation values of Zn(II)-bound hydroxide in CA cannot be determined directly by pH titration or ITC because there are many overlapping ionizing groups in proteins. Therefore, the pK_a is determined indirectly by modeling the U-shape dependence of the affinity on pH and the X-shape observed enthalpy dependence on pH (Fig. 4). The enthalpy of the hydroxide protonation is also determined from the model of the observed enthalpy dependence on pH in two buffers of different protonation enthalpy (Fig. 4).

The binding of EZA, measured by ITC in two buffers, phosphate (Pi) and TRIS, demonstrated the dependence of the observed binding enthalpy $\Delta_b H_{obs}$ on the buffer (Fig. 4a). The binding parameters strongly depended on the buffer pH as well, both for EZA and for TFS binding (Fig. 4b, c). Fitting of the observed experimental data obtained in TRIS and Pi buffers by applying Eq. (4) yielded the intrinsic binding enthalpy (horizontal dashed line). Fitting of the data enabled the determination of the pK_a of CA IV, which was equal to 7.0.

Another useful technique for the estimation of pK_a of the Zn(II)-bound water form of CA IV is FTSA. Figure 4d shows the dependence of the observed binding affinity on pH. The resulting U-shape of pH dependence can be approximated by Eq. (1). The value of pK_a for the Zn(II)-bound water form of CA IV used for fitting the U-shape was 6.5, a value which is slightly lower than that obtained by ITC technique. The intrinsic Gibbs energy for EZA binding was equal to −53.6 kJ/mol.

Characterization of CA IV stability by FTSA

FTSA was used to identify buffer conditions (pH ranges from 5 to 10) that stabilized CA IV. Different additives (salt

Table 2 The observed dissociation constants of selected compounds for all catalytically active human CA isoforms, determined by the fluorescent thermal shift assay at pH 7.0 and 25 °C

Compound	K_{d_obs} (nM)											
	CA I	CA II	CA III	CA IV	CA VA	CA VB	CA VI	CA VII	CA IX	CA XII	CA XIII	CA XIV
5	0.017	0.83	6670	170	100	0.020	50	0.45	2.0	17	0.63	2.0
18	500	10	11,100	18	1250	2.5	33	1.7	0.050	2.5	2.5	1.1
19	4000	10	33,300	1.0	1050	40	590	3.6	2.0	3.8	130	2.5
20	5000	290	100,000	200	670	630	250	67	130	330	100	20
26	670	33	2200	29	40	250	100	29	25	77	56	4.0
BSA	2860	1110	200,000	5560	2860	12,500	5000	2860	500	5560	3570	3330
AZM	714	13	16,700	50	500	25	83	8.3	14	71	25	22

The K_d for compounds **5**, **18**, and **26** binding to CA I, II, VII, XII, and XIII are taken from our previously published data, recalculated to 25 °C (Dudutienė et al. 2013, 2015; Čapkauskaitė et al. 2013; Zubrienė et al. 2017). Binding data for **19** and **20** are reported here for the first time

substances, glycerol, DMSO) and EZA inhibitor concentrations were used to examine a stabilizing or destabilizing effect on CA IV. The stability of CA IV was affected by pH, buffer, and the presence of various salts (Fig. 5). The protein was most stable at pH 8.0–8.5 (Fig. 5a, b). CA IV at pH 8.0 was more stable in Pi and HEPES buffers than in TRIS and carbonate buffers. Destabilization of CA IV by carbonate at pH 8–10 and by citrate buffer at pH 4.5–6.0 was observed. These buffers may have to be avoided in CA IV purification or storage.

Regular salts such as sodium chloride, sodium sulfate, and ammonium sulfate had different influences on the stability of CA IV. Sodium sulfate exhibited the greatest stabilization effect on the protein—the addition of 1 M sulfate increased the protein T_m by about 5 °C. Sodium chloride had a minor effect on CA IV stability, whereas the addition of ammonium sulfate slightly decreased protein T_m, primarily because it diminished the pH of the protein solution (Fig. 5c).

Both glycerol and DMSO had a minor destabilizing effect for CA IV (Fig. 5d). At 5–10% (v/v) of glycerol, the protein stability decreased by about 1 °C. The addition of DMSO at these concentrations destabilized the protein by about 2 °C.

Intrinsic thermodynamics of ligand binding

In order to calculate the intrinsic binding parameters by Eq. (1), the protonation parameters of both protein and sulfonamide are necessary. The pK_as of most tested sulfonamides were previously determined (Zubrienė et al. 2015; Linkuviene et al. 2016). The pK_a of the sulfonamide group for compound **19** was measured spectrophotometrically by measuring absorption at different pHs. The pK_as of **20**, **27**, and **32** were determined by analogy with other meta- and para-substituted benzenesulfonamides. We have recently shown that only the head-groups but not the tail groups on benzenesulfonamides influenced the ionization constants (Kišonaitė et al. 2014), thus the pK_a for meta substituted compounds **20** and **27** with chlorine atoms were 8.9, and for *para*-substituted benzenesulfonamide **32** was 9.4. The thermodynamic parameters of protonation of the deprotonated inhibitor sulfonamide group and the CA-Zn(II)-bound hydroxide anion, determined by ITC at 25 °C, are listed in Table 5.

The intrinsic $K_{d\text{-}intr}$ for synthesized compounds **1**–**35** and for reference compounds are listed in Table 1. The intrinsic $K_{d\text{-}intr}$ for all compounds was significantly higher than the observed dissociation constants. It is evident that the lower the value of pK_a for sulfonamide, the smaller the difference between the intrinsic and the observed dissociation constants (Fig. 6a, b). The largest differences between the observed and intrinsic K_d values were observed for compounds **34**, **35**, and BSA, where the binding to CA IV differed more than 8300-fold. The most tightly binding inhibitor, according to both the observed and intrinsic K_ds, was compound **19**, where the intrinsic K_d reached 3.6 pM, whereas the observed K_d was equal to 1.0 nM. Since the pK_a of TFS was equal to 6.3, the lowest among the tested compounds, the intrinsic K_d value for TFS was closest to the observed ($K_{d\text{-}intr}/K_{d\text{-}obs} = 3.3$).

The enthalpy-entropy compensation graph (Fig. 6c) shows that the intrinsic Gibbs energy of binding for the tested series of compounds (listed in Table 6) spreads over 24 kJ/mol, whereas the $\Delta\Delta_b H_{int}$ varies by 38 kJ/mol and $T\Delta\Delta_b S_{intr}$ by 50 kJ/mol. There is no clear enthalpy-entropy compensation and the enthalpy and entropy contribution to binding affinity is favorable, except for AZM, for which the large negative enthalpy ($\Delta_b H_{int} = -50.6$ kJ/mol) is slightly opposed by the negligible entropy contribution ($T\Delta_b S_{intr} = -3.7$ kJ/mol). EZA, TPM, AZM, MTZ and compound **26** bound to CA IV with the dominant enthalpy contribution, whereas compounds **5**, **18**, **19** and **20**—with the dominant favorable entropy. Favorable entropy and

Table 3 X-ray crystallographic data collection and refinement statistics

Names of inhibitors:	Compound **20**	Acetazolamide	Ethoxzolamide	Topiramate	4-Aminomethylbenzenesulfonamide	Methazolamide
Abbreviation:		AZM	EZA	TPM	PAMBS	MZM
Concentration (mM):	0.4	20	3	14	20	20
Buffer/salt	100 mM MES, pH 6.5/200 mM $(NH_4)_2SO_4$	100 mM Na acetate, pH 4.6/200 mM $(NH_4)_2SO_4$	100 mM Na acetate, pH 4.6/200 mM $(NH_4)_2SO_4$	100 mM Na acetate, pH 4.6/200 mM $(NH_4)_2SO_4$	100 mM Na acetate, pH 4.6/200 mM $(NH_4)_2SO_4$	100 mM Na acetate, pH 4.6/200 mM $(NH_4)_2SO_4$
PEG (%)	2000(20)	4000(21)	3350(16)	4000(21)	3350(16)	4000(23)
PDB ID	5IPZ	5JN8	5JN9	5JNA	5JNC	5KU6
Data collection						
Wavelength (Å)	0.83	1.54	1.54	1.54	1.54	1.54
Space group	$P2_1$	$P2_12_12_1$	$P2_12_12_1$	$P2_12_12_1$	$P2_12_12_1$	$P2_12_12_1$
Unit cell dimensions (Å)	$a = 48.7$ $b = 256.4$ $c = 48.6$ $\beta = 117.3°$	$a = 64.9$ $b = 123.5$ $c = 151.2$	$a = 64.8$ $b = 124.0$ $c = 151.3$	$a = 64.9$ $b = 123.8$ $c = 151.4$	$a = 64.8$ $b = 123.8$ $c = 151.4$	$a = 65.0$ $b = 123.7$ $c = 151.4$
Molecules/asymmetric unit	4	4	4	4	4	4
Resolution range (Å)	40–2.1	40–1.85	40–2.1	40–2.0	40–2.0	40–1.8
Observations		466,257	225,442	375,127	268,928	484,979
Unique observations	51,979	102,801	68,006	80,516	80,221	110,310
Completeness (%)	85.0 (77.0)	98.5 (96.8)	94.5 (93.4)	96.8 (92.7)	96.5 (90.9)	97.3 (94.2)
R_{sym} (%)	4.9 (41.7)	11.3 (47.4)	10.8 (46.4)	9.6 (42.4)	11.4 (43.4)	8.9 (42.2)
I/σ(I)	10.5 (2.1)	10.2 (2.0)	8.1 (1.9)	12.1 (2.4)	8.0 (2.0)	11.4 (2.1)
Refinement						
Resolution (Å)	40–2.1	40–1.85	40–2.1	40–2.0	40–2.0	40–1.8
R_{cryst}, R_{free}	0.225, 0.306	0.185, 0.228	0.170, 0.220	0.172, 0.218	0.174, 0.218	0.184, 0.216
Reflections (working/test)	46,821/5105	97,258/5127	64,559/3413	76,157/4002	76,144/4039	104,356/5481
Protein atoms	8252	8391	8376	8392	8376	8376
Zn^{++} ions/inhibitors	4/3	4/4	4/4	4/4	4/4	4/4
Solvent molecules	120	962	916	888	937	915
RMSD bond lengths[a] (Å)	0.012	0.010	0.013	0.010	0.012	0.009
RMSD angles[a] (°)	1.7	1.3	1.8	1.3	1.6	1.4
RMSD ΔB ($Å^2$) (mm/ms/ss)	3.43/3.23/3.70	1.49/1.54/2.25	1.90/2.23/2.96	1.44/1.46/2.34	1.62/1.88/2.51	1.36/1.48/2.27
<B > protein ($Å^2$)	50.5	20.8	28.9	26.5	24.0	21.0
<B > Zn^{++}/inhibitors ($Å^2$)	32.3/47.2	12.2/27.0	19.6/27.2	16.9/22.2	15.5/34.2	12.9/31.3
<B > solvent ($Å^2$)	41.8	32.6	38.5	38.8	36.2	33.8
Ramachandran plot						
Most favored (%)	90	100	100.0	100	100	100

Table 3 (continued)

Names of inhibitors:	Compound **20**	Acetazolamide	Ethoxzolamide	Topiramate	4-Aminomethylbenzenesulfonamide	Methazolamide
Abbreviation:		AZM	EZA	TPM	PAMBS	MZM
Concentration (mM):	0.4	20	3	14	20	20
Generously allowed (%)	9.8	0	0	0	0	0
Disallowed (%)	0.2	0	0	0	0	0

mm main chain–main chain, *ms* main chain-side chain, *ss* side chain-side chain

[a]Root-mean-squared deviation (RMSD) from ideal bond lengths and angles and RMSD in B-factors of bonded atoms

enthalpy contributions to binding affinity, in almost equal magnitudes, were observed for TFS.

The results presented here show that binding of CA IV to sulfonamides was significantly influenced by the composition of the buffer and its pH. The pK_a and ionization enthalpy of the Zn(II)-bound water molecule in the active site of CA IV were determined due to the EZA and TFS titrations at various pHs of TRIS and Pi buffers. Measurement of the binding affinity at various pHs by FTSA helped validate the pK_a values as well. When the pK_a and the enthalpy of protonation of sulfonamide and protein, as well as the enthalpy of buffer protonation, are known, the intrinsic thermodynamic parameters can be calculated and correlated with the high-resolution protein–ligand crystal structures. It was necessary to determine the pKa and enthalpy of protontion of the water molecule bound to Zn only once. When this has been accomplished here, future researchers can use these values in the calculation of the intrinsic parameters of any other sulfonamide ligand binding. A single determination at a single pH in a known buffer will be sufficient to calculate the intrinsic parameters. Such information may be valuable for further drug design of more effective and selective compounds. These known values enabled us to calculate the intrinsic binding values even from a single ITC titration experiment in a buffer with known protonation enthalpy and at a known pH (Table 6).

Conclusions

The observed binding affinity and the binding enthalpy of EZA to CA IV are pH-dependent. The pH dependence of the observed thermodynamic parameters shows the contributions of linked protonation-deprotonation reactions of both ligand and protein. The dissection of binding linked reactions yielded the intrinsic thermodynamic parameters, describing the reaction between the Zn-bound water form of CA IV and the anionic form of sulfonamide. The dominant intrinsic enthalpy contributed favorably to the Gibbs energy of EZA binding, whereas TFS binding was driven by entropy and enthalpy in equal parts. CA IV was most stable at pH 8.0–8.5. High sodium sulfate concentrations significantly stabilized the protein. Sodium chloride had insignificant effect on protein stability. High-resolution crystal structures for compound **20**, EZA, and PAMBS in complex with CA IV revealed the most important hydrophobic interactions between the ligand and the protein. The structure of residues 126–138 in human CA IV was a loop conformation and was very flexible. There were four different conformations in the segment. Although the conformations in this segment were different, all of them made the active site pocket bigger and allowed larger inhibitors to interact with the active site. This conformation is a unique feature of CA IV in the CA family.

Experimental section

Chemical compounds

EZA, AZM, TPM, MZM, TFS, and PAMBS were purchased from Sigma-Aldrich (St. Louis, MO, USA). The synthesis, chemical structural characterization, and the purity of compounds **1**–**35** has been previously described (Dudutienė et al. 2013, 2015; Čapkauskaitė et al. 2013; Zubrienė et al. 2014), with the exception of **19**, **20**, **27**, and **32**.

Synthesis of 19, 20, 27, and 32

All starting materials and reagents were commercial products and were used without further purification. The melting points of the synthesized compounds were determined in open capillaries on a Thermo Scientific 9100 Series apparatus without further correction. IR spectra were obtained on a Perkin-Elmer FT-IR spectrophotometer Spectrum BX II in KBr. ^{1}H and ^{13}C NMR spectra were recorded on a Varian Unity Inova (300 and 75 MHz, respectively) or Bruker

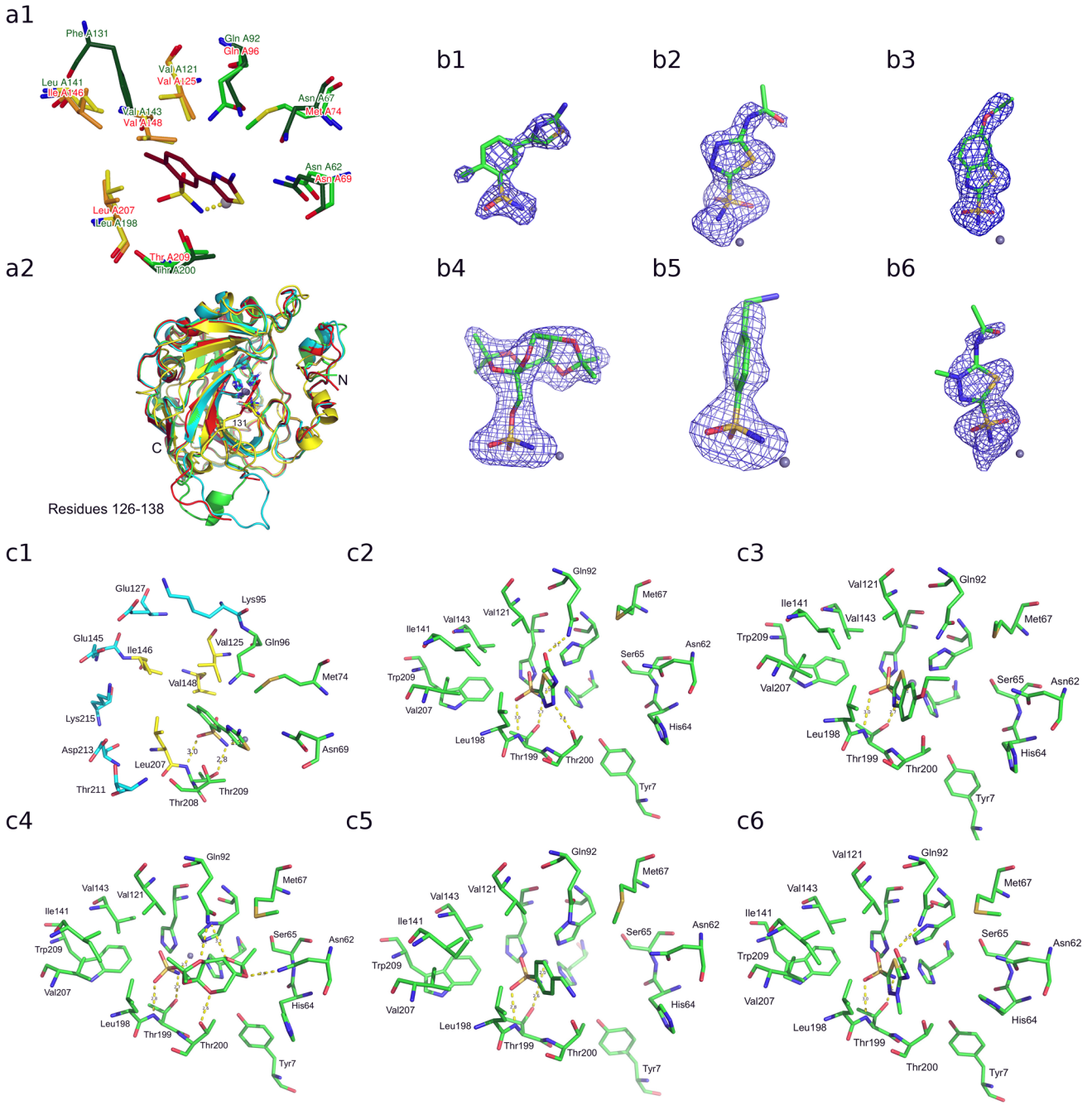

(400 and 100 MHz, respectively) spectrometers in DMSO-d_6 using residual DMSO signals (2.52 and 40.21 ppm for ^{1}H and ^{13}C NMR spectra, respectively) as the internal standard. TLC was performed with silica gel 60 F254 aluminum plates (Merck, Kenilworth, NJ, USA) and visualized with UV light. High-resolution mass spectra (HRMS) were recorded on a Dual-ESI Q-TOF 6520 mass spectrometer (Agilent Technologies, Santa Clara, CA, USA). The purity of final compounds was verified by HPLC to be > 95% using the Agilent 1290 Infinity instrument with a Poroshell 120 SB-C18 (2.1 mm × 100 mm, 2.7 µm) reversed-phase column. Analytes were eluted using a linear gradient of water/methanol (20 mM ammonium formate in both phases) from 60:40 to 30:70 over 12 min, then from 30:70 to 20:80 over 1 min, and then 20:80 over 5 min at a flow rate of 0.2 mL/min. UV detection was at 254 nm.

Compound **19a**, 2,4-dichloro-5-sulfamoyl-benzoic acid, was converted to chloroanhydride, then subjected to amidation of the acid choride with 3-aminopropan-1-ol to produce the amide, compound **19b**. Compound **19b** was then treated to esterification with ethylacetate to produce compound **19c**, 3-[(2,4-dichloro-5-sulfamoyl-benzoyl)amino]

◂**Fig. 3** X-ray crystallographic structures of compounds in complex with CA IV. (a1) The overlay of the binding sites of CA IV and CA II. The residues important for 2-chlorobenzene ring binding are colored yellow (CA IV) and orange (CA II). The residues that interact with compound **20** in CA IV are colored green and the spatially corresponding residues of CA II are colored dark green. The red and dark green labels belong to CA IV and CA II residues, respectively. (a2) Comparison for the structures: molecule C in complex with AZM (green), molecule A in the PDB entry 1ZNC, first crystal structure of CA IV at 2.8 Å resolution (blue), molecule A in complex with compound **20** (red), and human CA II (PDB ID: 4HTO, yellow, residue 131 is shown). The orientation of residues 126–138 in CA IV differs from CA II. The structure of residues 126–138 in CA II is very similar to other members of the CA family, in which residue 131 was an important residue located in a short helix and interacted with inhibitors in most CA family. This helix acts as a lid and closes the active site pocket in CA II. The structures of residues 126-138 in human CA IV were flexible and there were four different conformations (including a disordered one) in the four observed molecules. Although the conformations in this region were different, all of them made the active site pocket bigger and allowed larger inhibitors to interact with the active site. (b1) The electron density of compound **20** in the active site of human CA IV (expressed in *E. coli*). The electron density map |Fobs-Fcalc| was calculated after removing the coordinates of compound **20** from the model and contoured at 3.0 σ. (b2) Electron density map |Fo-Fc| after removing the coordinates of AZM from the model, contoured at 2.2 σ. (b3) The electron density map |Fo-Fc| after removing the coordinates of EZA from the model, contoured at 3.0 σ. (b4) The electron density map |Fo-Fc| after removing the coordinates of TPM from the model, contoured at 3.0 σ. (b5) The electron density map |Fo-Fc| after removing the coordinates of PAMBS from the model, contoured at 3.0 σ. (b6) The electron density map |Fo-Fc| after removing the coordinates of MZM from the model, contoured at 2.5 σ. (c) The binding mode of compounds in the active site of CA IV. The Zn(II) atom is shown as a pink sphere. The residues forming the hydrophilic area are colored aquamarine. (c1) Interactions between compound **20** and CA IV. The chlorine atom of chlorobenzene in **20** is located in the hydrophobic area of the CA IV active site (residues colored yellow). This hydrophobic area is conservative for human CA active sites (Alterio et al. 2012) and the binding mode of the chlorobenzene ring is common for CA XII, XIII, and II. Selected other residues of active site are shown in green. (c2) Interactions between AZM and protein (molecule D), hydrogen bonds are shown as dashed lines and Zn^{++} is shown as a pink sphere. (c3) Interactions between EZA and protein (molecule D), hydrogen bonds are shown as dashed lines and Zn(II) is shown as a pink sphere. (c4) Interactions between TPM and protein (molecule B), hydrogen bonds are shown as dashed lines and Zn(II) is shown as a pink sphere. (c5) Interactions between PAMBS and protein (molecule C), hydrogen bonds are shown as dashed lines and Zn(II) is shown as a pink sphere. (c6) Interactions between MZM and protein (molecule A), hydrogen bonds are shown as dashed lines and Zn^{++} is shown as a pink sphere

propyl acetate. Finally, compound **19c** was converted to compound **19**, 3-[(4-chloro-2-phenylsulfanyl-5-sulfamoyl-benzoyl)amino]propyl acetate, via nucleophilic substitution of the choride with thiophenol (Scheme 1).

2,4-Dichloro-N-(3-hydroxypropyl)-5-sulfamoyl-benzamide (19b)

The mixture of 2,4-dichloro-5-sulfamoylbenzoic acid (**19a**) (2.70 g, 10.0 mmol), $SOCl_2$ (3.57 g, 30.0 mmol), and 1 drop DMF in toluene (5 ml) was refluxed for 4 h. Excess $SOCl_2$ and toluene were removed by distillation under reduced pressure, and the crude acid chloride was used directly in the next step. The solution of 2,4-dichloro-5-sulfamoylbenzoyl chloride in THF (30 ml) was added dropwise to a solution of 3-aminopropan-1-ol (2.25 g, 30.0 mmol) in THF (20 ml) at 0 °C and allowed to stirr for 1 h. The mixture was warmed to room temperature and stirred for another 2 h. THF was removed under reduced pressure. Water was added to the residue and product was extracted with EtOAc. The organic layer was washed with 5% HCl(aq), dried over anhydrous $MgSO_4$, filtered, and concentrated. Yield was 60%, mp 153–155 °C (H_2O). ^{1}H NMR (400 MHz) δ ppm: 1.67 (2H, quint, J = 6.4 Hz, CH_2), 3.30 (2H, q, J = 6.4 Hz, NH$\underline{CH_2}$), 3.48 (2H, t, J = 6.4 Hz, $\underline{CH_2}$OH), 4.49 (1H, br *s*, OH), 7.83 (2H, *s*, SO_2NH_2), 7.92 (1H, s, C_3-H), 7.94 (1H, s, C_6-H), 8.65 (1H, t, J = 5.6 Hz, NH). ^{13}C NMR (100 MHz) δ ppm: 32.6, 36.9, 58.9, 129.2, 132.1, 132.5, 134.4, 136.4, 140.4, 164.9. HRMS calculated for $C_{10}H_{12}Cl_2N_2O_4S$ [$(M + H)^+$]: 326.9968, found: 326.9971.

3-[(2,4-Dichloro-5-sulfamoyl-benzoyl)amino]propyl acetate (19c)

2,4-Dichloro-*N*-(3-hydroxypropyl)-5-sulfamoyl-benzamide (**19b**) (327 mg, 1.00 mmol) was refluxed in EtOAc (7 mL) with 3 drops of concentrated H_2SO_4 for 2 h. The reaction mixture was concentrated under reduced pressure and the resultant precipitate was washed with H_2O. Yield: 288 mg, 78%, mp 149-151 °C. ^{1}H NMR (400 MHz) δ ppm: 1.83 (2H, quint, J = 6.4 Hz, CH_2), 2.02 (3H, s, CH_3), 3.30 (2H, q, J = 6.8 Hz, NH$\underline{CH_2}$), 4.08 (2H, t, J = 6.4 Hz, $\underline{CH_2}$O), 7.81 (2H, s, SO_2NH_2), 7.93 (1H, s, C_3-H), 7.95 (1H, s, C_6-H), 8.71 (1H, t, J = 5.6 Hz, NH). ^{13}C NMR (100 MHz) δ ppm: 21.2, 28.5, 36.5, 62.1, 129.1, 132.2, 132.5, 134.4, 136.1, 140.2, 164.9, 170.9. HRMS calculated for $C_{12}H_{14}Cl_2N_2O_5S$[$(M + H)^+$]: 369.0073, found: 369.0071.

3-[(4-Chloro-2-phenylsulfanyl-5-sulfamoyl-benzoyl)amino] propyl acetate (19)

The mixture of 3-[(2,4-dichloro-5-sulfamoyl-benzoyl) amino]propyl acetate (**19c**) (250 mg, 0.677 mmol), MeOH (5 mL), thiophenol (82.1 mg, 0.745 mmol), and Et_3N (82.2 mg, 0.813 mmol) was refluxed for 3 h. MeOH was evaporated under reduced pressure and the resultant precipitate was washed with H_2O. Yield 39%, mp 168–171 °C (toluene:2-PrOH (8:1)). ^{1}H NMR (400 MHz) δ ppm: 1.86 (2H, quint, J = 6.4 Hz, CH_2), 2.03 (3H, s, CH_3), 3.32–3.36 (2H, m, NH$\underline{CH_2}$), 4.10 (2H, t, J = 6.4 Hz, $\underline{CH_2}$O), 6.82 (1H, s, C_3-H), 7.55–7.56 (5H, m, Ph-H), 7.64 (2H, s, SO_2NH_2), 8.01 (1H, s, C_6-H), 8.81 (1H, t, J = 5.2 Hz, NH). ^{13}C NMR (100 MHz) δ ppm: 21.2, 28.6, 36.7, 62.3, 128.6, 129.6,

Table 4 Buried surface areas calculated by PISA v1.06 (Krissinel and Henrick 2007) of amino acid side chains that interact with **20**. Data presented for the protein chain A

Aa of active site	TRP 6	ASN 69	HIS 71	SER 72	MET 74	GLN 96	HIS 98	HIS 100	HIS 123	VAL 125	ILE 146	VAL 148	LEU 207	THR 208	THR 209	TRP 218
Buried surface area (Å^2)	5.78	19.93	9.99	4.86	18.80	15.52	19.60	1.09	1.69	8.57	1.68	3.34	26.80	6.20	29.95	3.44

130.4, 130.8, 131.4, 132.3, 133.6, 135.2, 138.0, 144.6, 166.0, 170.9. HRMS calculated for $C_{18}H_{19}ClN_2O_5S_2[(M + H)^+]$: 443.0497, found: 443.0495.

5-(2-Aminothiazol-4-yl)-2-chloro-benzenesulfonamide (**20**) and 3-(4-chloro-3-methyl-phenyl)-5,6-dihydro-2*H*-imidazo[2,1-b]thiazol-3-ol **(27)** were obtained using the same reaction conditions from 5-(2-bromoacetyl)-2-chlorobenzenesulfonamide (**20a**) and thioureas (Scheme 2).

S-Alkylation of phenylmethanethiol with 5-(bromoacetyl)-2-chlorobenzenesulfonamide (**32a**) to give 4-(2-benzylsulfanylacetyl)benzenesulfonamide (**32**) was carried out in the presence of sodium acetate in tetrahydrofuran at room temperature (Scheme 3).

Synthesis of (**20a**) was accomplished from commercially available 1-(4-chloro-3-nitrophenyl)ethanone as reported previously (Oelschlager 1961), Fujikura et al. 1982). 4-(bromoacetyl)benzenesulfonamide (**32a**) was synthesized from commercially available 1-(4-aminophenyl)ethanone as described in (Fujikura et al. 1982).

General procedure for the synthesis of 20, 27, and 32

A mixture of corresponding bromoacetophenone **20a, 32a** (0.360 mmol), appropriate thioureas or phenylmethanethiol (0.704 mmol), and NaOAc (63.0 mg, 0.768 mmol) in THF (3 ml) was stirred at room temperature for 24 h. The reaction mixture was poured into water. The precipitate was filtered off, washed with water, and then with Et_2O.

5-(2-Aminothiazol-4-yl)-2-chloro-benzenesulfonamide (20)

Yield 82%, mp 235-237 °C. IR ν cm^{-1}: 3444, 3353, 3257 (NH_2). ^{1}H NMR (300 MHz) δ, ppm: 7.20 (3H, s, NH_2, $C_{5'}$-H), 7.62 (2H, s, SO_2NH_2), 7.63 (1H, d, J = 8.1 Hz, C_3-H), 7.99 (1H, dd, J = 8.4 Hz, J = 2.1 Hz, C_4-H), 8.46 (1H, d, J = 2.1 Hz, C_6-H). ^{13}C NMR (75 MHz) δ, ppm: 104.3, 126.8, 129.2, 130.2, 132.3, 134.7, 141.9, 148.2, 169.3. HRMS calculated for ($C_9H_8ClN_3O_2S_2$): [(M + H)$^+$]: 289.9819, found: 289.9819.

3-(4-Chloro-3-methyl-phenyl)-5,6-dihydro-2H-imidazo[2,1-b]thiazol-3-ol (27)

Yield 80%, mp 158–160 °C. ^{1}H NMR (300 MHz) δ, ppm: 2.96–3.19 (2H, m, NCH_2), 3.69 (1H, d, J = 11.7 Hz, SCH_2), 3.79 (1H, d, J = 11.7 Hz, SCH_2), 3.91–4.12 (2H, m, NCH_2), 7.10 (1H, br s, OH), 7.69–7.72 (3H, m, C_3-H, NH_2), 7.77 (1H, dd, J = 1.8 Hz, J = 8.1 Hz, C_4-H), 8.20 (1H, d, J = 1.8 Hz, C_6-H). ^{13}C NMR (75 MHz) δ, ppm: 42.9, 49.8, 61.4, 87.8, 127.5, 131.0, 131.8, 132.5, 141.7, 142.0, 170.4. HRMS calculated for ($C_{11}H_{12}ClN_3O_3S_2$): [(M + H)$^+$]: 334.0081, found: 334.0084.

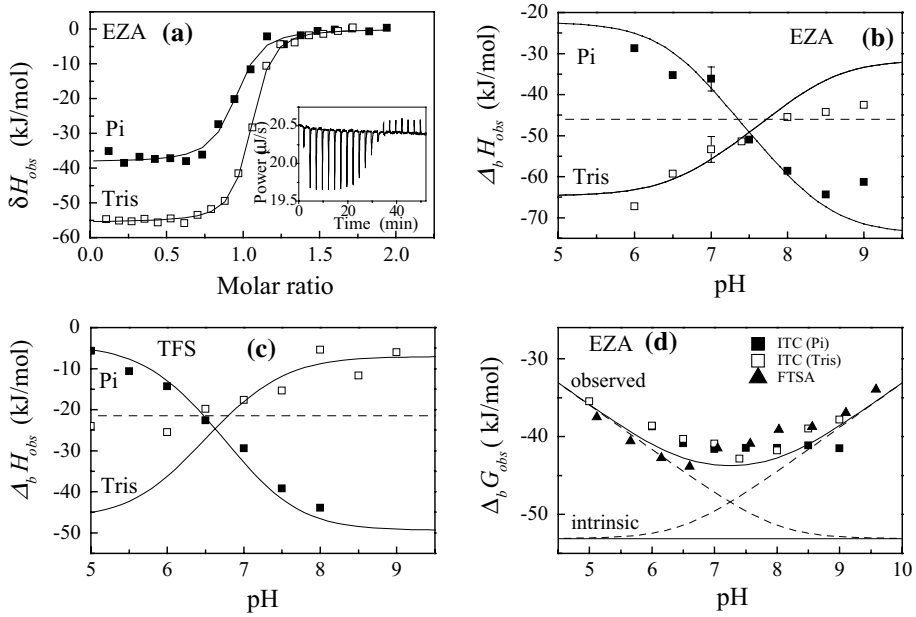

Fig. 4 The dependence of sulfonamide inhibitor binding to CA IV as a function of pH. **a** The observed enthalpies of EZA binding to CA IV in sodium phosphate (filled square) and TRIS chloride (open square) buffer, both at pH 7.0, 25 °C, determined by the ITC. Panels **b**, **c** show the observed enthalpies of EZA, **b** and TFS **c** binding to CA IV in sodium phosphate (filled square) and TRIS chloride (open square) buffers (at 25 °C, as a function of pH). Data points represent the observed enthalpies obtained by ITC, while the curves were fit according to Eq. (4). **d** The observed and intrinsic Gibbs energies of EZA binding to CA IV as a function of pH. Datapoints show $\Delta_b G_{obs}$ obtained by ITC in phosphate (filled square) and TRIS (open square) buffers and by FTSA in the universal buffer (filled triangle). Solid bent line is the fit according to Eq. (1) recalculated to Gibbs energies. Dashed lines show the contributions of the fractions of deprotonated EZA and protonated CA IV. The straight horizontal line shows the intrinsic Gibbs free energy of EZA binding that is independent of pH

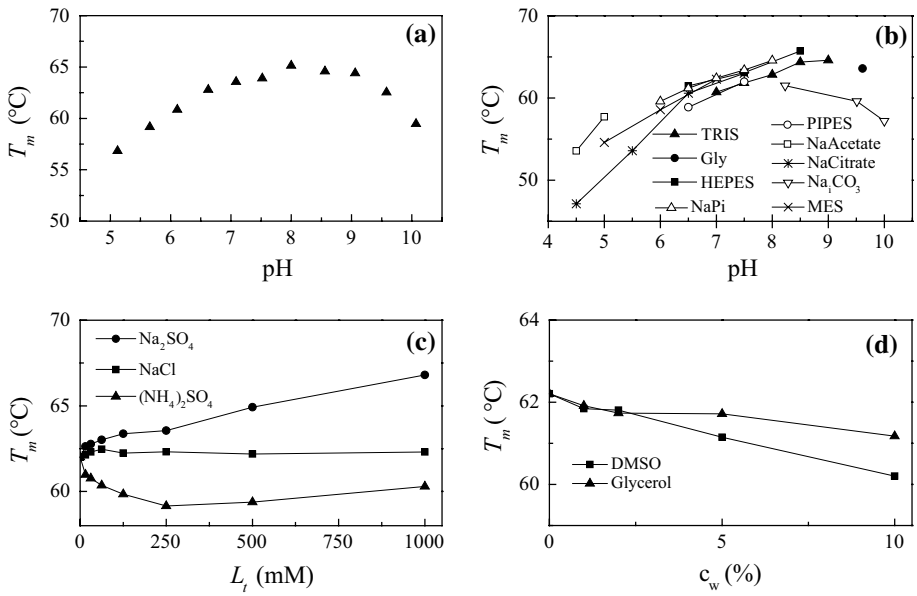

Fig. 5 Thermal stability of CA IV in various buffers, pHs, and salts. **a** CA IV melting temperature (T_m) dependence on pH of universal buffer. **b** CA IV melting temperature (T_m) dependence on pH in various buffers (100 mM): sodium acetate (NaAcetate, open square), sodium citrate (NaCitrate, asterisk), sodium phosphate (NaPi, open triangle), sodium carbonate ($NaCO_3$, open down triangle), glycine (Gly, filled circle), TRIS (filled triangle), MES (multiplication), HEPES (filled triangle), and PIPES (open circle). **c** The melting temperature of CA IV as a function of various salt concentrations: $(NH_4)_2SO_4$ (filled triangle), Na_2SO_4 (filled circle), and NaCl (filled square). **d** CA IV stability at various added concentrations of DMSO (filled square) and glycerol (filled triangle)

Table 5 The thermodynamic parameters of protonation of the deprotonated inhibitor sulfonamide group and the CA–Zn(II)-bound hydroxide anion, determined by ITC at 25 °C

Inhibitor/protein	PK_a	ΔG_{prot} (kJ/mol)	ΔH_{prot} (kJ/mol)	$T\Delta S_{prot}$ (kJ/mol)
5[a]	8.3	−47.4	−28.9	18.5
18[b]	8.0	−45.7	−26.8	18.9
19	9.0	−51.4	−30.1	21.3
20	8.9	−50.8	−26.8	24.0
26[c]	8.9	−50.8	−26.8	24.0
EZA[d]	8.0	−45.7	−29.5	16.2
TFS[d]	6.3	−36.0	−22.4	13.6
AZM[e]	7.3	−41.7	−23.0	18.7
MZM[b]	7.1	−40.5	−25.1	15.4
PAMBS[b]	10.1	−57.7	−23.0	34.6
TPM	8.7[f]	−49.7	−29.3	20.4
CA IV–Zn–H_2O	6.8	−38.8	−33.0	5.8

[a]Data taken from (Zubrienė et al. 2015), [b](Zubrienė et al. 2017), [c](Kišonaitė et al. 2014), [d](Jogaitė et al. 2013), [e](Matulis and Todd 2004), [f](Maryanoff et al. 1998)

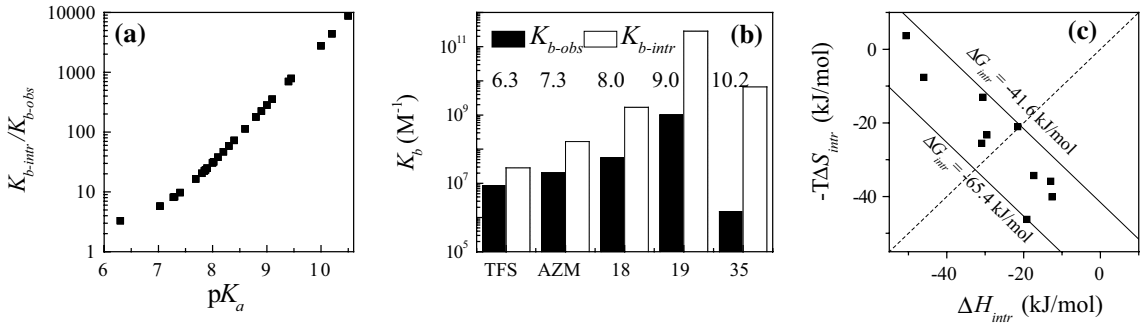

Fig. 6 Comparison between the *observed* binding constants and the *intrinsic* affinities. Only the intrinsic values should be used for the drawing of compound structure–affinity correlations. **a** Dependence of the $K_{b\text{-}int}/K_{b\text{-}obs}$ ratio on the compound pK_a. The ratio of binding constants increases with the pK_a. **b** The intrinsic (black column) and observed (white column) K_b values of compounds with different pK_a values 6.3, 7.3, 8.0, 9.0, and 10.2. **c** The intrinsic enthalpy–entropy compensation plot for compound binding to CA IV. Diagonal lines represent the Gibbs energies (solid upper line −41.6 kJ/mol, equivalent to 100 nM K_d, solid bottom line −65.4 kJ/mol equivalent to 0.01 nM K_d)

Table 6 The intrinsic thermodynamic parameters of compound binding to CA IV, determined by ITC at 25 °C

Inhibitor	$\Delta_b H_{intr}$ (kJ/mol)	K_{b_intr} (M^{-1})	$\Delta_b G_{intr}$ (kJ/mol)	$T\Delta_b S_{intr}$ (kJ/mol)
5	−12.9	2.5×10^7	−48.8	35.9
18	−12.5	2.8×10^8	−52.7	40.1
19	−19.1	6.7×10^9	−65.3	46.2
20	−17.3	2.1×10^7	−51.6	34.3
26	−30.9	1.7×10^8	−56.5	25.6
EZA	−46.0	2.5×10^9	−53.6	7.6
TFS	−21.5	2.8×10^7	−42.5	21.0
AZM	−50.6	1.7×10^8	−46.9	−3.7
MZM	−30.6	4.4×10^7	−43.6	13.0
PAMBS	ND	1.1×10^9	−51.5	ND
TPM	−29.9	3.1×10^9	−54.2	24.3

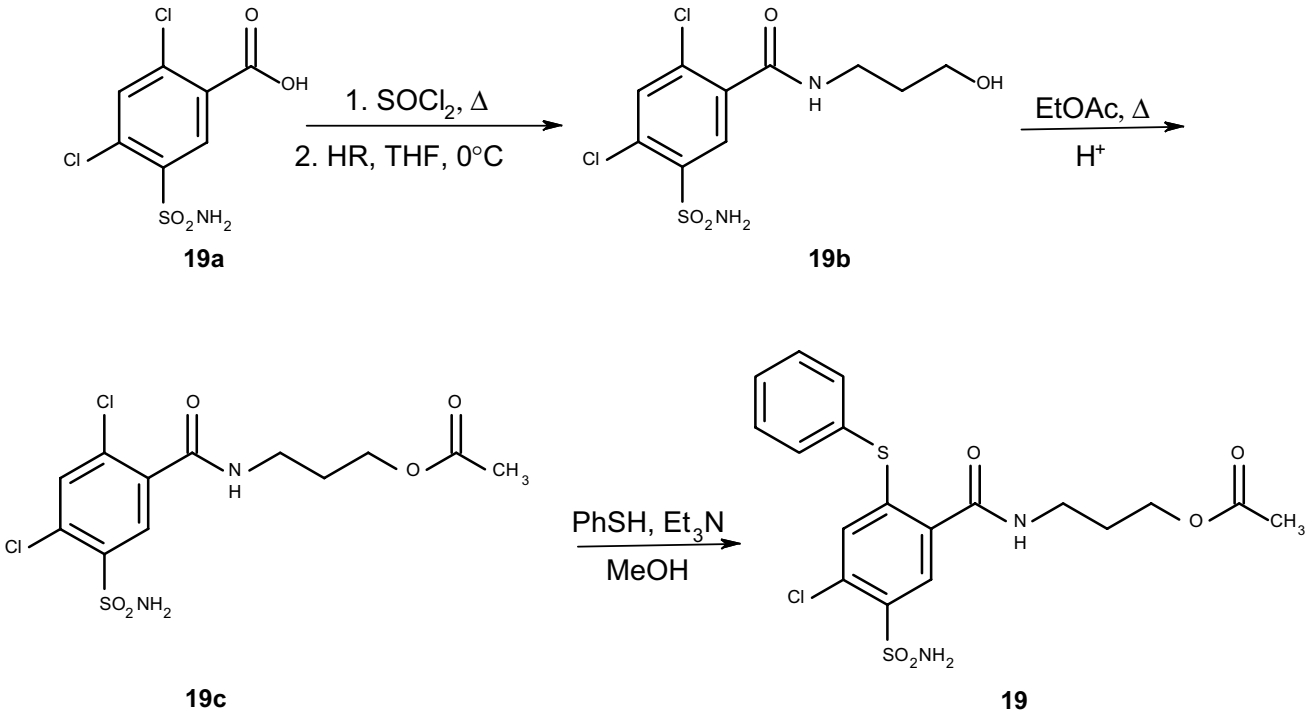

Scheme 1 Synthesis of compound **19**

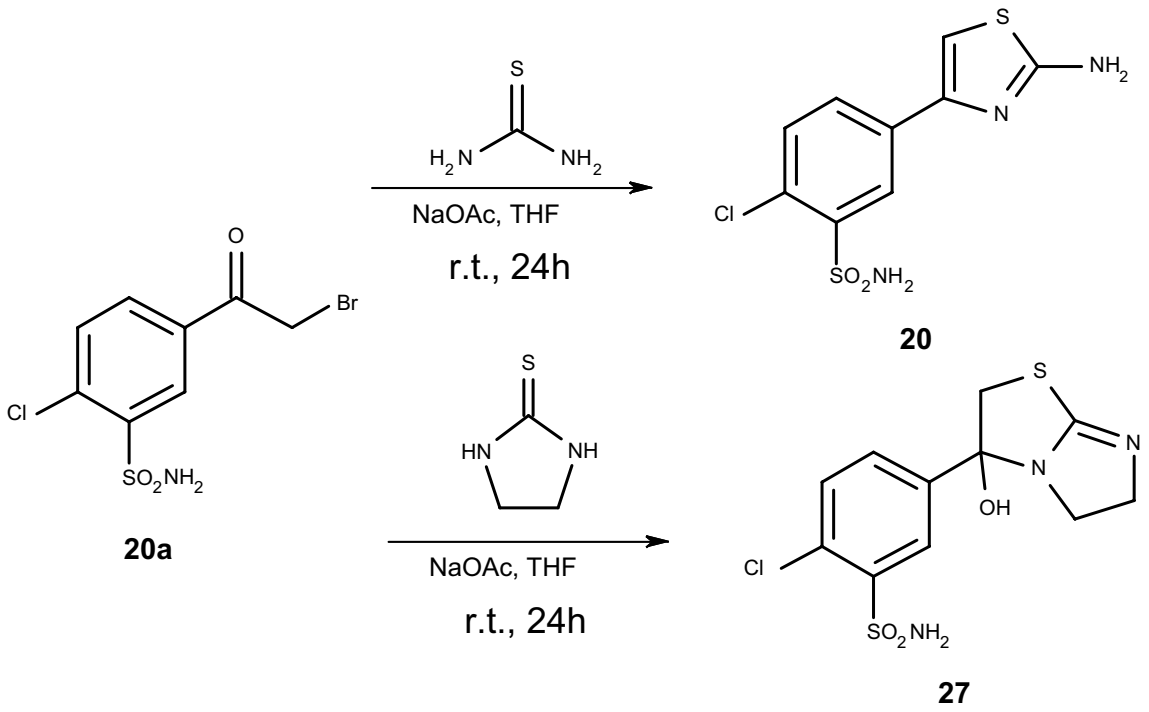

Scheme 2 Synthesis of compounds **20** and **27**

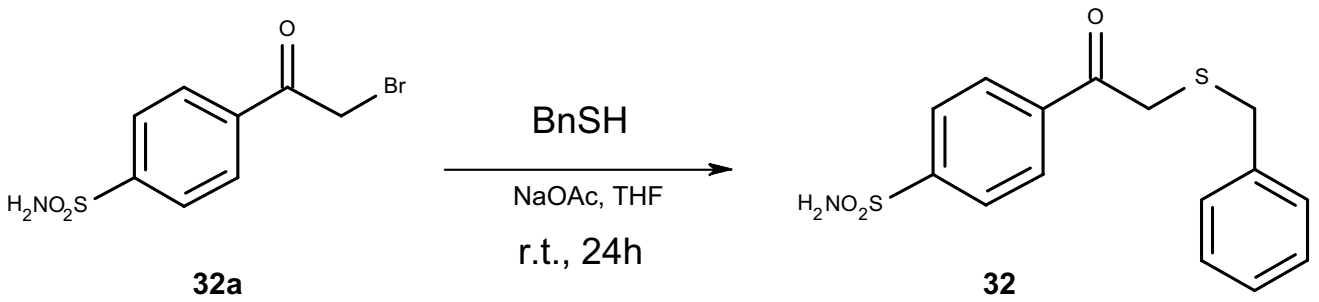

32a **32**

Scheme 3 Synthesis of the compound **32**

4-(2-Benzylsulfanylacetyl)benzenesulfonamide (32)

Yield 82%, mp 155-157 °C, IR ν cm^{-1}: 3382, (NH_2), 1690 (CO). ^{1}H NMR δ, ppm: 3.74 (2H, s, SCH_2), 3.96 (2H, s, CH_2CO), 7.24–7.29 (1H, m, $C_{4'}$-H), 7.33–7.40 (4H, m, $C_{2',3',5',6'}$-H), 7.59 (2H, s, NH_2), 7.96 (2H, d, J = 8.4 Hz, $C_{2,6}$-H), 8.15 (2H, d, J = 8.7 Hz, $C_{3,5}$-H). ^{13}C NMR δ, ppm: 35.9, 37.3, 126.6, 127.8, 129.2 (2C), 129.8, 130.0, 138.3, 148.5, 194.6. HRMS calculated for ($C_{15}H_{15}NO_3S_2$): [$(M + H)^+$]: 322.0566, found: 322.0562.

Production of recombinant CA IV

The cDNA of CA IV was purchased from RZPD Deutsches Ressourcenzentrum für Genomforschung (Berlin, Germany). The gene encoding the catalytic domain of human CA IV (19–284 aa) was expressed in *Escherichia coli* Origami^{TM} B (DE3) (Novagen, EMD Millipore, Billerica, MA, USA) cells. The transformed colony was transferred to BHI (Brain Heart Infusion) medium containing 60 μM $ZnSO_4$ and the cells were cultivated at 37 °C until reaching 0.6–0.7 OD_{600}. Then 0.5 mM $ZnSO_4$ was added and protein expression was induced with 1 mM isopropyl β-D-1-thiogalactopyranoside (IPTG). The cells were grown for 20 h at 16 °C. The biomass was harvested by centrifugation at 4000×*g* for 20 min at 4 °C.

Mammalian CA IV (19–284 aa) was produced as previously described (Dudutiene et al. 2014).

The pellet was suspended in the lysis buffer (20 mM HEPES, 0.15 M NaCl, pH 8.0) containing 1× protease inhibitor cocktail (Roche Applied Science, Indianapolis, IN, USA) and 1 mM PMSF (SERVA, Heidelberg, Germany). The cells were incubated by mixing at 4 °C for 60 min and then sonicated for 15 min, 70% amplitude, using 1/1 min intervals. The supernatant was separated by centrifugation at 30,000×*g* for 25 min at 4 °C. Supernatant was mixed with *p*-aminomethylbenzene sulfonamide-agarose (Sigma-Life Science Aldrich) and left to incubate overnight slightly shaken at 4 °C. The next day, CA IV (19–284 aa) was purified using a CA-affinity column containing the mentioned sorbent. Elution buffer contained 0.1 M sodium acetate, 0.5 M $NaClO_4$, pH 5.6. Eluted protein was dialyzed into a buffer containing 20 mM HEPES, 20 mM NaCl, pH 8. After dialysis, CA IV (19–284 aa) was further purified using an anion exchange column with Q Sepharose^{TM} Fast Flow (GE Healthcare, Little Chalfont, United Kingdom). Protein was eluted with 20 mM HEPES, 1 M NaCl, pH 8. Eluted protein was dialyzed into a storage buffer containing 20 mM HEPES, 50 mM NaCl, pH 7.5, and stored at −80 °C.

CA IV (19–284 aa) purity was confirmed using SDS–PAGE. Concentration was measured by the Bradford method. The molecular weight of the purified CA IV (19–284 aa) was measured by HRMS and was 30,320.74 Da, nearly equal to the theoretical molecular weight calculated from the amino acid sequence minus Met without water (30,323.4 Da). The difference in weight of 2 Da occurs due to the possible reduction–oxidation of Cys found in CA IV (19–284 aa).

Human CA IV was purified using CA-inhibitor affinity resins as described (Waheed et al. 1996). Post affinity enzyme was dialyzed against 10 mM Tris–Sulfate pH 7.5 or 10 mM ammonium bicarbonate pH 8.0. Dialyzed enzyme was lyophilized for storage at 4 °C. Quality of the enzyme was assessed by SDS–PAGE and by measuring the specific activities. This CA IV preparation was used to obtain the crystal structures with AZM, MZM, PAMBS, EZA, and TPM. Both CA IV preparations gave specific activity of 3000–4000 EU/mg.

Compound binding to CA IV by isothermal titration calorimetry (ITC)

ITC measurements were performed using the iTC_{200} instrument (Microcal, Inc., Northampton, MA, USA, now part of Malvern Instruments Ltd., UK). Protein solution (10 μM in the cell, volume 200 μl) was titrated with the compound solution in the syringe (100 μM, 40 μl). A typical experiment consisted of 19 injections, 2 μL each, with 2–3 min intervals between injections. Experiments were performed at 25 °C in 50 mM TRIS chloride or sodium phosphate buffers

containing 100 mM NaCl and 0.5-2% DMSO concentrations both in the cell and syringe. Protein stock solutions were dialyzed against the buffers that were used to prepare the ligand solutions. ITC data were analyzed using MicroCal Origin software. The first point obtained using the 0.5 µL injection in the integrated data graph was deleted. The binding constants and the enthalpies and entropies of binding were estimated after fitting the data with the single binding site model.

The enthalpy of TPM deprotonation was measured using VP-ITC instrument. Inhibitor (0.25 mM) was deprotonated by adding 1.3 equivalent of NaOH and titrated with 2.5 mM HNO_3. The experiment consisted of 58 injections (5 µl each) added at 4 min intervals. Experiment was performed at 25 °C with 0.5% of DMSO, equal in the syringe and the cell.

Compound binding to CA IV by the fluorescent thermal shift assay (FTSA)

During the FTSA experiments, the protein solution was heated from room temperature to 99 °C while following the extrinsic fluorescence of a solvatochromic probe, such as 1,8-anilinonaphthalene sulfonate (ANS), that strongly changes its fluorescence upon protein unfolding (Stryer 1965; Slavik et al. 1982; Matulis and Lovrien 1998; Matulis et al. 1999). The thermal melting temperatures (T_m) are strongly dependent on the ligand binding affinity and concentration as previously described (Brandts and Lin 1990; Matulis et al. 2005; Cimmperman et al. 2008). FTSA experiments were performed with a Corbett Rotor-Gene 6000 (QIAGEN Rotor-Gene Q) instrument using the blue channel (excitation 365 ± 20, detection 460 ± 15 nm), applying the heating rate of 1 °C/min. Usually the samples contained 20 µL of 10 µM protein, 0–400 µM ligand, 50 µM 8-anilino-1-naphthalene sulfonate, 50 mM sodium phosphate at pH 7.0, 50 mM NaCl, and 2% DMSO. The pH dependence of the observed binding constant (K_b) was determined in the buffer containing 50 mM sodium phosphate, 50 mM sodium acetate, 25 mM sodium borate, and 50 mM NaCl, pH 5.0–10.0. The FTSA data was fit and analyzed as previously described (Cimmperman et al. 2008).

Intrinsic thermodynamics of compound binding to CA IV

Several linked reactions occur during sulfonamide inhibitor binding to CA that prevent direct determination of the intrinsic affinity, namely, the zinc-bound hydroxide ion protonation in the active center of the CA, the ligand sulfonamide group deprotonation, a coordination bond formation between the protein and deprotonated sulfonamide amine, and finally, the compensating protonation–deprotonation of the buffer. Each of these reactions contributes to the observed binding parameters, the binding constant, and the enthalpy of binding.

The intrinsic binding constant K_{b_intr} is equal to the observed binding constant K_{b_obs} divided by the available fractions of deprotonated inhibitor and protonated Zn(II)-bound water form of CA

$$K_{b\_intr} = \frac{K_{b\_obs}}{(f_{RSO_2NH^-} f_{CAZnH_2O})}. \quad (1)$$

The fractions of the deprotonated inhibitor and the Zn-bound water form of CA can be calculated if both pK_a values of the sulfonamide (pK_{a_sulf}) and the CA (pK_{a_ZnH2O}) are known:

$$f_{RSO_2NH^-} = \frac{10^{pH-pK_{a\_sulf}}}{1 + 10^{pH-pK_{a\_sulf}}}, \quad (2)$$

$$f_{CAZnH_2O} = 1 - \frac{10^{pH-pK_{a\_ZnH_2O}}}{1 + 10^{pH-pK_{a\_ZnH_2O}}}. \quad (3)$$

The observed enthalpy is the sum of all protonation events and the intrinsic binding reaction itself. Linked reactions that have to be subtracted are the protonation of the zinc-bound hydroxide ion in the active center of CA, deprotonation of sulfonamide, and the protonation/deprotonation of the buffer:

$$\Delta_b H_{intr} = \Delta_b H_{obs} - n_{sulf}\Delta_{b\_proton\_sulf}H - n_{CA}\Delta_{b\_proton\_CA}H + n_{buf}\Delta_{b\_proton\_buf}H, \quad (4)$$

where $\Delta_b H_{obs}$ is the observed binding enthalpy, $n_{sulf} = f_{RSO_2NH^-}$ is the number of protons binding to the inhibitor, $\Delta_{b\_proton\_sulf}H$ is the enthalpy of inhibitor protonation, $n_{CA} = 1 - f_{CAZnH_2O}$ is the number of protons bound to the Zn-hydroxide, $\Delta_{b\_proton\_CA}H$ is the enthalpy of CA protonation, $n_{buf} = n_{sulf} + n_{CA}$, is the net sum of taken up or released protons, and $\Delta_{b\_proton\_buf}H$ is the buffer protonation enthalpy. The enthalpy of TRIS protonation is equal to −47.45 kJ/mol and the enthalpy of phosphate buffer protonation is equal to −5.1 kJ/mol at 25 °C (Goldberg and Lennen 2002).

Crystallization, X-ray diffraction data collection, and structure determination

The crystallization buffer contained 0.2 M ammonium sulfate, 0.1 M sodium MES (pH 6.5) and 20% PEG2000 methylmonoester, and crystals were obtained by crystallization of a mixture of CA IV (25 mg/ml) with 0.4 mM of compound **20** for the complex of CA IV and compound **20**. For the other five complexes of CA IV and inhibitors, 8 mg/ml CA

IV in 50 mM Tris sulfate, pH 8.0 and 2 mM benzamidine were mixed with 3–20 mM inhibitors (Table 1) before crystallization. Crystals were grown by the hanging drop vapor diffusion technique using an Art Robbins Instruments (Sunnyvale, CA, USA) Phoenix liquid handling robot in a solution of 100 mM Na acetate, pH 4.6, 200 mM ammonium sulfate, and 16–23% PEG 4000 or PEG 3350 (Table 1). Crystals were grown in 1–2 weeks at 277 K and were cryoprotected in a solution containing mother liquid and 15% glycerol prior to flash freezing. Data were collected at the EMBL P14 beamline at the PETRAIII storage ring, DESY, Hamburg (Germany) for the complex with compound **20**. Data for other complexes were collected with a home source (Rigaku 1.2 kw MMX007 generator with VHF optics) Rigaku Raxis IV^{++} detector. All data were collected at 100 K.

Datasets for the complex with compound **20** were processed by MOSFLM (Leslie 2006) and other datasets were indexed, integrated, and scaled with the HKL2000 software package (Otwinowski and Minor 1997). All structures were solved by molecular replacement using the MOLREP program (Vagin and Teplyakov 1997). The initial phases were received from PDB entry 3F7B for the complex with compound **20** and PDB entry 1ZNC for other complexes. For the complex with compound **20**, 3D models of inhibitors were created using the molecule editor AVOGADRO (Hanwell et al. 2012). The chemical and geometric descriptions of inhibitors used in refinement were generated by LIBCHECK CCP4 (Collaborative Computational Project, N. 4 1994). For other complexes, the models of inhibitors were obtained from Protein Data Bank. A model of PAMBS was obtained from RCS (Triscarbonyl-cyclopentadienyl-4-aminomethylbenzene sulfonamide) and the Triscarbonyl-cyclopentadienyl was removed. The chemical and geometric descriptions for these inhibitors were generated automatically by REFMAC (Murshudov et al. 1997). Refinement and electron density generation were performed with REFMAC (Murshudov et al. 1997). Ten and 5% of the reflections were randomly selected as test sets for cross-validation for the complex with compound **20** and other complexes, respectively. Model building and analysis of the structures were carried out using COOT (Emsley and Cowtan 2004). In the final refinement stage, TLS tensors modeling rigid-body anisotropic temperature factors were calculated and applied to the models except for the complexes with compound **20**, EZA, and PAMBS. Ramachandran plots were calculated using PROCHECK (Morris et al. 1992). Statistics for data collection and refinement are summarized in Table 3. Atomic coordinates and structure factors have been deposited in Protein Data Bank (accession codes 5IPZ, 5JN8, 5JN9, 5JNA, 5JNC, and 5KU6 for the complexes with compound **20**, AZM, EZA, TPM, PAMBS, and MZM, respectively).

PDB IDs: 5IPZ—**20**, 5JN8—AZM, 5JN9—EZA, 5JNA—TPM, 5JNC—PAMBS, and 5KU6—MZM. Authors will release the atomic coordinates and experimental data upon article publication.

Acknowledgements This research was funded by the Grant SEN-04/2015 from the Research Council of Lithuania to J.M. and by National Institutes of Health Grants HL049413 and HL073813 to E.D.C. The authors also acknowledge the COST projects CM1406, CM1407, CA15126, and CA15135. The authors are grateful to Gleb Burenkov for assistance with data collection at EMBL P14 beamline at the PETRA III storage ring, DESY Hamburg. The authors also thank Tracey Baird for editorial assistance in the preparation of this manuscript.

References

Alterio V, Fiore AD, D'Ambrosio K, Supuran CT, Simone GD (2012) Multiple binding modes of inhibitors to carbonic anhydrases: how to design specific drugs targeting 15 different isoforms? Chem Rev 112:4421–4468

Baird JTT, Waheed A, Okuyama T, Sly WS, Fierke CA (1997) Catalysis and inhibition of human carbonic anhydrase IV. Biochemistry 36:2669–2678

Balaydin HT, Senturk M, Menzek A (2012) Synthesis and carbonic anhydrase inhibitory properties of novel cyclohexanonyl bromophenol derivatives. Bioorg Med Chem Lett 22:1352–1357

Barker H, Aaltonen M, Pan P, Vähätupa M, Kaipiainen P, May U, Prince S, Uusitalo-Järvinen H, Waheed A, Pastoreková S, Sly WS, Parkkila S, Järvinen TA (2017) Role of carbonic anhydrases in skin wound healing. Exp Mol Med 49:e334

Brandts JF, Lin LN (1990) Study of strong to ultratight protein interactions using differential scanning calorimetry. Biochemistry 29:6927–6940

Breton S (2001) The cellular physiology of carbonic anhydrases. JOP 2:159–164

Cammer W, Zhang H, Tansey F (1995) Effects of carbonic anhydrase II (CAII) deficiency on CNS structure and function in the myelin-deficient CAII-deficient double mutant mouse. J Neurosci Res 40:451–457

Čapkauskaitė E, Zubrienė A, Smirnov A, Torresan J, Kišonaitė M, Kazokaitė J, Gylytė J, Michailovienė V, Jogaitė V, Manakova E, Gražulis S, Tumkevičius S, Matulis D (2013) Benzenesulfonamides with pyrimidine moiety as inhibitors of human carbonic anhydrases I, II, VI, VII, XII, and XIII. Bioorg Med Chem 21:6937–6947

Christie KN, Thomson C, Xue L, Lucocq JM, Hopwood D (1997) Carbonic anhydrase isoenzymes I, II, III, and IV are present in human esophageal epithelium. J Histochem Cytochem 45:35–40

Cimmperman P, Baranauskienė L, Jachimovičiūtė S, Jachno J, Torresan J, Michailovienė V, Matulienė J, Sereikaitė J, Bumelis V, Matulis D (2008) A quantitative model of thermal stabilization and destabilization of proteins by ligands. Biophys J 95:3222–3231

Collaborative Computational Project, N. 4 (1994) The CCP4 suite: programs for protein crystallography. Acta Cryst D 50:760–763

Datta R, Waheed A, Bonapace G, Shah GN, Sly WS (2009) Pathogenesis of retinitis pigmentosa associated with apoptosis-inducing mutations in carbonic anhydrase IV. Proc Natl Acad Sci USA 106:3437–3442

Datta R, Shah GN, Rubbelke TS, Waheed A, Rauchman M, Goodman AG, Katze MG, Sly WS (2010) Progressive renal injury from transgenic expression of human carbonic anhydrase IV folding mutants is enhanced by deficiency of p58IPK. Proc Natl Acad Sci USA 107:6448–6452

Del Prete S, Vullo D, Fisher GM, Andrews KT, Poulsen S-A, Capasso C, Supuran CT (2014) Discovery of a new family of carbonic anhydrases in the malaria pathogen Plasmodium falciparum—the η-carbonic anhydrases. Bioorg Med Chem Lett 24:4389–4396

Dudutiene V, Matuliene J, Smirnov A, Timm DD, Zubriene A, Baranauskiene L, Morkunaite V, Smirnoviene J, Michailoviene V, Juozapaitiene V et al (2014) Discovery and characterization of novel selective inhibitors of carbonic anhydrase IX. J Med Chem 57:9435–9446

Dudutienė V, Zubrienė A, Smirnov A, Gylytė J, Timm D, Manakova E, Gražulis S, Matulis D (2013) 4-Substituted-2,3,5,6-tetrafluorobenzenesulfonamides as inhibitors of carbonic anhydrases I, II, VII, XII, and XIII. Bioorg Med Chem 21:2093–2106

Dudutienė V, Zubrienė A, Smirnov A, Timm DD, Smirnovienė J, Kazokaitė J, Michailovienė V, Zakšauskas A, Manakova E, Gražulis S, Matulis D (2015) Functionalization of fluorinated benzenesulfonamides and their inhibitory properties toward carbonic anhydrases. ChemMedChem 10:662–687

Elleuche S, Pöggeler S (2010) Carbonic anhydrases in fungi. Microbiology 156:23–29

Emsley P, Cowtan K (2004) Coot: model-building tools for molecular graphics. Acta Crystallogr D 60:2126–2132

Ferrari S, Di Iorio E, Barbaro V, Ponzin D, Sorrentino FS, Parmeggiani F (2011) Retinitis pigmentosa: genes and disease mechanisms. Curr Genomics 12:238–249

Ferry JG (2010) The gamma class of carbonic anhydrases. Biochim Biophys Acta 1804:374–381

Fujikura T, Miigata K, Hashimoto S, Imai K, Takenaka T (1982) Studies on benzenesulfonamide derivatives with alpha- and beta-adrenergic antagonistic and antihypertensive activities. Chem Pharm Bull 30:4092–4101

Goldberg RMRN, Lennen Kishore N (2002) Thermodynamic quantities for the ionization reactions of buffers. J Phys Chem Ref Data 31:231–370

Hanwell MD, Curtis DE, Lonie DC, Vandermeersch T, Zurek E, Hutchison GR (2012) Avogadro: an advanced semantic chemical editor, visualization, and analysis platform. J Cheminform 4:17

Innocenti A, Villar R, Martinez-Merino V, Gil MJ, Scozzafava A, Vullo D, Supuran CT (2005) Carbonic anhydrase inhibitors: inhibition of cytosolic/tumor-associated carbonic anhydrase isozymes I, II, and IX with benzo[b]thiophene 1,1-dioxide sulfonamides. Bioorg Med Chem Lett 15:4872–4876

Jogaitė V, Zubrienė A, Michailovienė V, Gylytė J, Morkūnaitė V, Matulis D (2013) Characterization of human carbonic anhydrase XII stability and inhibitor binding. Bioorg Med Chem 21:1431–1436

Kikutani S, Nakajima K, Nagasato C, Tsuji Y, Miyatake A, Matsuda Y (2016) Thylakoid luminal θ-carbonic anhydrase critical for growth and photosynthesis in the marine diatom Phaeodactylum tricornutum. Proc Natl Acad Sci USA 113:9828–9833

Kišonaitė M, Zubrienė A, Čapkauskaitė E, Alexey S, Smirnovienė Joana V, Kairys V, Michailovienė E, Manakova S Gražulis, Matulis D (2014) Intrinsic thermodynamics and structure correlation of benzenesulfonamides with a pyrimidine moiety binding to carbonic anhydrases I, II, VII, XII, and XIII. PLoS ONE 9:e114106

Kivelä A-J, Kivelä J, Saarnio J, Parkkila S (2005) Carbonic anhydrases in normal gastrointestinal tract and gastrointestinal tumours. World J Gastroenterol 11:155–163

Köhn L, Burstedt MSI, Jonsson F, Kadzhaev K, Haamer E, Sandgren O, Golovleva I (2008) Carrier of R14 W in carbonic anhydrase IV presents Bothnia dystrophy phenotype caused by two allelic mutations in RLBP1. Invest Ophthalmol Vis Sci 49:3172–3177

Krishnamurthy VM, Kaufman GK, Urbach AR, Gitlin I, Gudiksen KL, Weibel DB, Whitesides GM (2008) Carbonic anhydrase as a model for biophysical and physical-organic studies of proteins and protein-ligand binding. Chem Rev 108:946–1051

Krissinel E, Henrick K (2007) Inference of macromolecular assemblies from crystalline state. J Mol Biol 372:774–797

Lane TW, Saito MA, George GN, Pickering IJ, Prince RC, Morel FMM (2005) Biochemistry: a cadmium enzyme from a marine diatom. Nature 435:42

Leslie AGW (2006) The integration of macromolecular diffraction data. Acta Crystallogr D 62:48–57

Linkuviene V, Matuliene J, Juozapaitiene V, Michailoviene V, Jachno J, Matulis D (2016) Intrinsic thermodynamics of inhibitor binding to human carbonic anhydrase IX. Biochim Biophys Acta 1860:708–718

Liu R, Bu W, Xi J, Mortazavi SR, Cheung-Lau JC, Dmochowski IJ, Loll PJ (2012) Beyond the detergent effect: a binding site for sodium dodecyl sulfate (SDS) in mammalian apoferritin. Acta Crystallogr D 68:497–504

Maryanoff BE, Costanzo MJ, Nortey SO, Greco MN, Shank RP, Schupsky JJ, Ortegon MP, Vaught JL (1998) Structure-activity studies on anticonvulsant sugar sulfamates related to topiramate. Enhanced potency with cyclic sulfate derivatives. J Med Chem 41:1315–1343

Matulis D, Lovrien R (1998) 1-Anilino-8-naphthalene sulfonate anion-protein binding depends primarily on ion pair formation. Biophys J 74:422–429

Matulis D, Todd MJ (2004) Thermodynamics-structure correlations of sulfonamide inhibitor binding to carbonic anhydrase. In: Ladbury JE, Doyle ML (eds) Biocalorimetry 2. Wiley, Chichester, pp 107–132

Matulis D, Baumann CG, Bloomfield VA, Lovrien RE (1999) 1-anilino-8-naphthalene sulfonate as a protein conformational tightening agent. Biopolymers 49:451–458

Matulis D, Kranz JK, Salemme FR, Todd MJ (2005) Thermodynamic stability of carbonic anhydrase: measurements of binding affinity and stoichiometry using ThermoFluor. Biochemistry 44:5258–5266

McMurtrie HL, Cleary HJ, Alvarez BV, Loiselle FB, Sterling D, Morgan PE, Johnson DE, Casey JR (2004) The bicarbonate transport metabolon. J Enzyme Inhib Med Chem 19:231–236

Morris AL, MacArthur MW, Hutchinson EG, Thornton JM (1992) Stereochemical quality of protein structure coordinates. Proteins 12:345–364

Murshudov GN, Vagin AA, Dodson EJ (1997) Refinement of macromolecular structures by the maximum-likelihood method. Acta Crystallogr D 53:240–255

Nishimori I, Vullo D, Innocenti A, Scozzafava A, Mastrolorenzo A, Supuran CT (2005) Carbonic anhydrase inhibitors: inhibition of the transmembrane isozyme XIV with sulfonamides. Bioorg Med Chem Lett 15:3828–3833

Oelschlager H (1961) 3-Alkyl-6-Halogen-Aniline Aus p-Halogenierten Fettaromatischen Ketonen. Justus Liebigs Ann Chem 641:81–94

Otwinowski Z, Minor W (1997) Processing of x-ray diffraction data collected in oscillation mode. Methods Enzymol 276:307–326

Pastorekova S, Parkkila S, Pastorek J, Supuran CT (2004) Carbonic anhydrases: current state of the art, therapeutic applications and future prospects. J Enzyme Inhib Med Chem 19:199–229

Purkerson JM, Schwartz GJ (2007) The role of carbonic anhydrases in renal physiology. Kidney Int 71:103–115

Slavik J, Horak J, Rihova L, Kotyk A (1982) Anilinonaphthalene sulfonate fluorescence and amino acid transport in yeast. J Membr Biol 64:175–179

Stams T, Christianson DW (2000) X-ray crystallographic studies of mammalian carbonic anhydrase isozymes. Birkhäuser, Basel, pp 159–174

Stams T, Nair SK, Okuyama T, Waheed A, Sly WS, Christianson DW (1996) Crystal structure of the secretory form of membrane-associated human carbonic anhydrase IV at 2.8-Å resolution. Proc Natl Acad Sci USA 93:13589–13594

Sterling D, Alvarez BV, Casey JR (2002) The extracellular component of a transport metabolon. Extracellular loop 4 of the human AE1 Cl-/HCO3- exchanger binds carbonic anhydrase IV. J Biol Chem 277:25239–25246

Stryer L (1965) The interaction of a naphthalene dye with apomyoglobin and apohemoglobin. A fluorescent probe of non-polar binding sites. J Mol Biol 13:482–495

Supuran CT (2008) Carbonic anhydrases—an overview. Curr Pharm Des 14:603–614

Supuran CT (2004) Carbonic anhydrases: catalytic and inhibition mechanisms, distribution and physiological roles. In: Supuran CT, Scozzafawa A, Conway J (eds) Carbonic anhydrase–its inhibitors and activators. CRC Press, Boca Raton, pp 1–24

Svichar N, Waheed A, Sly WS, Hennings JC, Hübner CA, Chesler M (2009) Carbonic anhydrases CA4 and CA14 both enhance AE3-mediated Cl–HCO3- exchange in hippocampal neurons. J Neurosci 29:3252–3258

Tamai S, Waheed A, Cody LB, Sly WS (1996) Gly-63–>Gln substitution adjacent to His-64 in rodent carbonic anhydrase IVs largely explains their reduced activity. Proc Natl Acad Sci USA 93:13647–13652

Vagin A, Teplyakov A (1997) MOLREP: an automated program for molecular replacement. J Appl Cryst 30:1022–1025

Vernier W, Chong W, Rewolinski D, Greasley S, Pauly T, Shaw M, Dinh D, Ferre RA, Nukui S, Ornelas M, Reyner E (2010) Thioether benzenesulfonamide inhibitors of carbonic anhydrases II and IV: structure-based drug design, synthesis, and biological evaluation. Bioorg Med Chem 18:3307–3319

Waheed A, Okuyama T, Heyduk T, Sly WS (1996) Carbonic anhydrase IV: purification of a secretory form of the recombinant human enzyme and identification of the positions and importance of its disulfide bonds. Arch Biochem Biophys 333:432–438

Yang Z, Horton JR, Maunus R, Wilson GG, Roberts RJ, Cheng X (2005) Structure of HinP1I endonuclease reveals a striking similarity to the monomeric restriction enzyme MspI. Nucleic Acids Res 33:1892–1901

Zhang J, Tsoi H, Li X, Wang H, Gao J, Wang K, Go MY, Ng SC, Chan FK, Sung JJ, Yu J (2016) Carbonic anhydrase IV inhibits colon cancer development by inhibiting the Wnt signalling pathway through targeting the WTAP-WT1-TBL1 axis. Gut 65:1482–1493

Zolfaghari Emameh R, Barker HR, Syrjänen L, Urbański L, Supuran CT, Parkkila S (2016a) Identification and inhibition of carbonic anhydrases from nematodes. J Enzyme Inhib Med Chem 31:176–184

Zolfaghari Emameh R, Barker HR, Tolvanen MEE, Parkkila S, Hytönen VP (2016b) Horizontal transfer of β-carbonic anhydrase genes from prokaryotes to protozoans, insects, and nematodes. Parasit Vectors 9:152

Zubrienė A, Čapkauskaitė E, Gylytė J, Kišonaitė M, Tumkevičius S, Matulis D (2014) Benzenesulfonamides with benzimidazole moieties as inhibitors of carbonic anhydrases I, II, VII, XII and XIII. J Enzyme Inhib Med Chem 29:124–131

Zubrienė A, Smirnovienė J, Smirnov A, Morkūnaitė V, Michailovienė V, Jachno J, Juozapaitienė V, Norvaišas P, Manakova E, Gražulis S, Matulis D (2015) Intrinsic thermodynamics of 4-substituted-2,3,5,6-tetrafluorobenzenesulfonamide binding to carbonic anhydrases by isothermal titration calorimetry. Biophys Chem 205:51–65

Zubrienė A, Smirnov A, Dudutienė V, Timm DD, Matulienė J, Michailovienė V, Zakšauskas A, Manakova E, Gražulis S, Matulis D (2017) Intrinsic thermodynamics and structures of 2,4- and 3,4-substituted fluorinated benzenesulfonamides binding to carbonic anhydrases. ChemMedChem 12:161–176